91602
new 82-10

LEGAL NOTICE

This report was prepared by Ontario Hydro and, while effort has been made to assure the accuracy and applicability of the material contained herein, neither Ontario Hydro nor any person acting on its behalf:

(a) makes any warranty, express or implied with respect to the use of any information, apparatus, method or process disclosed in this report or that such use may not infringe privately owned rights; or

(b) assumes any liabilities with respect to the use of, or for damages resulting from the use of, any information, apparatus, method or process disclosed in this report.

ontario hydro
research division

VALIDATION ANALYSES OF THE CONCRETE INTEGRATED CONTAINER

Report No. 89-298-K

H.P. (Jack) Lee
Engineer
Applied Mechanics Section
Mechanical Department

ABSTRACT

Two finite element impact analyses to simulate 1/4 and 1/8 scale CIC (Concrete Integrated Container) model drop tests are performed. The purpose is to examine the accuracy of the analytical prediction through comparison against test results and to verify the suitability of using the hydrodynamic computer code DYNA3D to carry out analyses for the CIC. The engineering software package PATRAN is used to pre-process the two mathematical models and, after analyses, to post-process the resulting data including energy, contact force, stresses, strains and deformations. The impact response of the CIC is closely examined and compared with the experiments in terms of acceleration and deformation and found to be in agreement. It is concluded that the impact damage experienced by the CIC can be predicted accurately and the computer code DYNA3D is suitable to perform such analyses.

job	file	date	report no.
21-173-461	825.12	April 30, 1990	89-298-K

91602
new 82-10

90-06107/

ontario hydro
research division

EXECUTIVE SUMMARY

VALIDATION ANALYSES OF THE CONCRETE INTEGRATED CONTAINER

H.P. (Jack) Lee
Applied Mechanics Section
Mechanical Research Department

The use of a concrete integrated container (CIC) for interim dry storage and transportation of irradiated fuel is presently under investigation in Ontario Hydro. One of the main objectives in this investigation is to meet the regulatory requirement regarding the structural integrity of the container should an accidental drop occur during operation. Both theoretical analyses and experimental tests have subsequently been carried out considering the CIC undergoing a nine meter top-down corner drop onto a rigid target.

For the analysis, mathematical treatment to simulate such an impact scenario is complex and difficult. It involves transient dynamics, geometrical and material nonlinearities with finite deformation, stress wave propagation, various types of materials experiencing different modes of failure, establishment of proper constitutive laws, vulnerability to numerical instability during analysis and others. Application of the state-of-the-art technology is essential. For this reason, a bench mark analysis was first performed and has been reported earlier.

This report describes the two subsequent analyses to simulate the actual drop tests of the two scaled (1/4 and 1/8) CIC models. The objectives are to correlate the analysis with experiment, to verify the accuracy of the analytical prediction and to validate the computer code used in the analyses. The engineering software package PATRAN is first employed as a pre-processor to generate the two mathematical models. Then, the analyses are carried out by applying the finite element technique using the hydrodynamic computer code DYNA3D. After the analyses, PATRAN is again used to post-process the results by sorting, interpreting, summarizing and presenting various parameters including energy, contact force, stress, strains and deformations for closer examination.

It is concluded that the impact damage experienced by the CIC can be predicted accurately and the comuter code DYNA3D is suitable to perform such impact analyses.

RTH
JC

job	file	date	report no.
21-173-461	825.12	April 30, 1990	89-298-K

TABLE OF CONTENTS

		PAGE
1.0	INTRODUCTION	1
2.0	GEOMETRY OF THE SCALED CIC MODELS	2
3.0	GEOMETRY OF THE TARGET PAD	2
4.0	MATERIAL PROPERTIES	2
	4.1 Steel Liners	2
	4.2 Concrete	2
	4.2.1 Yield Model	3
	4.2.2 Equation of State	3
	4.3 Steel Reinforcement	3
5.0	FINITE ELEMENT MODELLING	4
6.0	ANALYTICAL RESULTS - CIC RESPONSES	4
	6.1 1/4 Scale Model	5
	6.2 1/8 Scale Model	6
7.0	COMPARISON BETWEEN 1/4 AND 1/8 SCALE MODELS	7
8.0	COMPARISON BETWEEN ANALYTICAL AND EXPERIMENTAL RESULTS	7
	8.1 1/4 Scale Model	7
	8.2 1/8 Scale Model	8
9.0	CONCLUSIONS	8
REFERENCES		10
TABLES		11
FIGURES		13
DISTRIBUTION		last page

ontario hydro
research division

To Mr. P.D. Stevens-Guille
Radioactive Materials Management
Nuclear Engineering Department
Design and Development Division

VALIDATION ANALYSES OF THE CONCRETE INTEGRATED CONTAINER

1.0 INTRODUCTION

The Nuclear Engineering Department is currently investigating the use of a reinforced concrete integrated container (CIC) for interim dry storage and transportation of irradiated fuel. One major consideration in this investigation is the assurance of its structural integrity in the event of an accidental drop of the container during operation. Subsequently, two separate approaches are undertaken to perform the study, namely: 1) experimental approach to carry out the actual physical drop of the container, 2) analytical approach to predict the response and damage of the CIC.

Models of 1/4 and 1/8 scale have recently been constructed and tested with and without impact limiters/1/. At the request of NED, two finite element impact analyses to simulate the two drops without impact limiters have been performed with the following objectives:

1. To provide detailed information for investigating the response of CIC's during impact.

2. To compare the analytical predictions for the two models with the test results.

3. To investigate the applicability of the Ontario Hydro's version of the computer code DYNA3D/2/ for CIC impact analysis.

This report describes the details of the analyses and summarizes their comparison.

2.0 GEOMETRY OF THE SCALED CIC MODELS

Basically the configuration of the container is a thick high-density concrete cylindrical tank with a lid. The concrete tank is enclosed by outer and inner steel liners. The lid is an inverted "hat" shaped structural component also self-enclosed with steel plates and filled with the same high density concrete. The lid is anchored to the concrete using ASTM A574 anchor bolts uniformly spaced around the circumference. Figures 1 and 2 are the typical cross section views with all dimensions, thickness and bolt size identified for the 1/4 and 1/8 scale model respectively/3,4/.

Figures 3 and 4 show the simulation of payload which was placed inside the container for the 1/4 scale and 1/8 scale models respectively. They are composed of a series of steel pipes with varied diameters. Gaps between the pipes were filled with regular concrete to achieve the proper scaled payload mass.

3.0 GEOMETRY OF THE TARGET PAD

The configuration of the target pad is shown in Figure 5 and is composed of two pieces of 1.83 m x 1.83 m x 0.2 m (6' x 6' x 8") steel plates and a piece of 2.5 m x 2.5 x 0.25 m concrete pad. The two steel plates are held together using a piece of 5" x 7" x 1" aluminum plate with six 1/2"ϕ anchor bolts on all four sides of the plates. The concrete pad is reinforced by steel wire mesh and is half buried in the ground. There is no physical link between the steel and concrete pad.

4.0 MATERIAL PROPERTIES

There are three different types of structural material involved: 1) The structural mild steel for the CIC liners, 2) the CIC high density concrete and 3) the steel reinforcement for the concrete. The mechanical properties used in the analyses for these materials are as follows:

4.1 Steel Liners

The steel liners are made of the conventional structural steel and the stress-strain relation is assumed as shown in Figure 6. Linear strain hardening is proposed in order to fit the input format of the computer code.

The properties of the steel liners are:

Density	ρ = 7,850 kg/m^3
Young's Modulus	E = 203 x 10^3 MPa
Poisson's Ratio	ν = 0.3
Yield Strength	σ_y = 370 MPa
Hardening Modulus	E_t = 0.5 x 10^3 MPa

4.2 Concrete

The concrete used for the CIC is a specially designed high density mix. Compression and tensile tests were performed by Civil Research/5/ specifically for the current 1/4 and 1/8 scale models. The test data is summarized in Table 1. Based on this data, the calculated concrete properties for computer input are:

Density	ρ = 3,535 kg/m^3
Shear Modulus	G = 20 x 10^3 MPa
Cut-off Pressure	P_{min} = 1.4 MPa

Two types of constitutive relations are required since the concrete is treated as a hydrodynamic material:

a) A model to define the failure of the concrete (yield criterion)
b) A model to describe the pressure-volume change relation (equation of state) of concrete.

They are described in the following:

4.2.1 Yield Model

Being a granular material, the yield strength of concrete has generally been treated based on the Mohr-Coulomb Model. This implies that the concrete strength depends on its subjected normal stress state (i.e., hydrostatic pressure). In other words, the higher the confined pressure, the greater the stress required to fail the material. This is because the higher confined pressure induces higher shear resistance which governs the yield condition.

To construct the current yield model, an inverse polynomial function with the following form is adopted:

$$\sigma_y^2 = a_0 + a_1 P$$

Where σ_y is the concrete yield strength and P is the hydrostatic pressure which is mathematically represented by the negative average of the three normal stress components. The constants a_0 and a_1, are subsequently obtained based on the data from the two tests (compression and tension) reported in Table 1 and the resulting yield model is shown in Figure 7.

4.2.2 Equation of State

Similar to other granular materials, the equation of state for concrete possesses the form shown in Figure 8. When subjected to pressure, concrete initially responds elastically until it is crushed at point A. Then the concrete engages in aggregate compaction resulting in reduced stiffness. The complete compaction is achieved at point B and thereafter concrete regains approximately its original strength against compression. It is assumed that the concrete experiences elastic unloading should the pressure decrease in the post-crush stage. Furthermore, concrete's response to tension (i.e., negative pressure) is limited by its tensile strength. Once this limit is reached, concrete is assumed to be cracked and its ability to resist tension drops to zero.

Because no equation of state test has been performed for the concrete, the piecewise linear model shown in Figure 9 is proposed for the analyses. This model is based on past experience.

4.3 Steel Reinforcement

The properties for concrete re-bar are based on CSA G20.16M 400 W which is equivalent to the previously-known Grade 60 billet steel. In accordance with ASTM, this steel possesses a minimum yield strength of 60 ksi and an ultimate strength of 90 ksi. A typical stress-strain curve for this grade of steel is shown in Figure 10. Again linear strain hardening is assumed to fit the input format of the computer code. The properties are summarized as follows:

Density	ρ	= 7850 kg/m^3
Young's Modulus	E	= 203 x 10^3 MPa
Poisson's Ratio	ν	= 0.3
Yield Strength	σ_y	= 450 MPa
Hardening Modulus	E_t	= 2.0 x 10^3 MPa

5.0 FINITE ELEMENT MODELLING

The scaled CIC structural system is transformed into a mathematical model through the interactive engineering software package PATRAN. As the finite element technique will be applied in the analyses, the CIC steel liners are simulated by four-noded shell elements and the concrete, payload and target pad by eight-noded solids. PATRAN, functioning as a pre-processor, creates these elements and generates a set input data for later analyses. Due to symmetry, only half of the CIC and target pad are modelled and analyzed.

Figure 11 illustrates the physical skeleton of the CIC and the target pad for the 1/4 scale model. The shell elements stimulating the steel liners and the solids for the concrete and payload with their positions relative to the target are demonstrated in Figures 12 and 13 respectively. A schematic finite element model of the system in color-filled form is provided in Figure 14 where the black represents shell elements while the blue represents solids. It should be noted that, because it is a top-down corner drop, it is the lid end of the CIC hitting the target pad.

Finite element generation for the 1/8 scale model is identical to that of 1/4 scale model except that the physical size of the CIC is smaller. Therefore, figures showing the detailed shell and solid element meshs, which are similar to Figures 12 and 13 respectively, are omitted. Only the physical skeleton of the system and its final finite element model in color-filled form are demonstrated in Figures 15 and 16 respectively.

For both the 1/4 and 1/8 scale models, there are outer layer and inner layer concrete reinforcing steels/6,7/. The steels are laid horizontally and vertically to form a mesh of reinforcement. This is modelled by shell elements with equivalent steel area per unit width. However, for the economy of modelling and computing, only the first quarter portion of the reinforcement most adjacent to the impact corner is modelled with the identical mesh pattern to that of outer and inner steel liners. The remaining three quarters of the reinforcement farther away from impacting corner are ignored.

6.0 ANALYTICAL RESULTS - CIC RESPONSE

The CIC system is assumed to undergo a nine (9) meter top-down corner drop with its C.G. (center of gravity) directly above the impact point. The formal stress analyses are carried out using the hydrodynamic code DYNA3D, an explicit three dimensional finite element code for analyzing the large deformation dynamic response of inelastic solids and structures. The analytical data is then fed back to PATRAN for post-processing. With its colour graphic capability, PATRAN sorts, interprets, summarizes and presents the resulting data in various suitable forms.

The results are reported and discussed in terms of energy, contact force, deformation, stress and strain. For stress, the effective stress (i.e., Von Mises stress in this case) is used to express the multi-stress state experienced in the CIC for simplicity. It also provides engineers with a direct comparison against material strength. For concrete, with its tensile strength significantly less than its compressive strength, hydrostatic pressure is reported to supplement the normal stress state of the material. All the stresses reported in the figures are in units of MPa. For strain, the equivalent plastic strain is reported. The area with the plastic strain indicates the severity of damage at any part of the CIC system.

6.1 1/4 Scale Model

Figures 17 shows the kinetic energy-time history of the CIC system during the impact. The figure shows a full stop at approximately 0.0052 second after initial contact, followed by a rebound. The smoothness of the curve implies a stable numerical analysis. Figure 18 provides the contact force time history between the CIC and the target pad during impact. It is noted that the peak force of about 23.8×10^5 Newtons is reached at approximate 0.004 second which is then chosen as the reference time for later presentation of stress and strain.

Figure 19 presents a complete picture of the final deformed CIC against the target pad. It can be seen that the deformation and damage is very much limited to the localized area in the vicinity of contact. Figure 20 gives a clear illustration in a larger scale with only the steel liners and reinforcements being plotted. The shape of the deformation in the outer liner and the consistent ident on reinforcing plates and inner liners due to the compression by concrete can be understood intuitively. The deformation of the cover plate for the CIC lid is shown in Figure 21. It is seen that only the flange at the contact region is warped.

Figures 22 and 23 show the effective stress on the outside and inside faces of the steel outer liner respectively. The figures indicate that there is no significant difference in the stress distribution pattern nor in the magnitude of the stress level. Figure 24 illustrates the stress in the inner liner.

The stress in the outer and inner layer of reinforcement are demonstrated in Figures 25 and 26 respectively. It can be seen that the highest stress occurs at the severely deformed corner of the outer layer reinforcement (see Fig. 25). This is because the steel plate representing the reinforcement is much thinner than the liners. The plate is subjected to higher stress when it is deformed within a small region causing severe curvature changes. It should be noted that higher stress is concentrated in the vicinity of the impacting corner and decreases rapidly toward remote area. It should also be remembered that Figures 25 and 26 only plot a quarter of the complete concrete reinforcement. Stress in the remaining three quarters of the reinforcement is smaller and becomes insignificant.

Figures 27 and 28 demonstrate the stress distribution in the liners and reinforcements at 0.004 second and 0.006 second respectively. It can be seen that, except at the severely deformed tip of the outer layer reinforcement where stress remains high, stress in the entire CIC has been significantly reduced due to the unloading being experienced from 0.004 second to 0.006 second.

Stress distribution in the cover plate of the CIC lid is provided in Figure 29. Again yielding is localized in the contact corner. It is interesting to observe that stress (in lower level) is passed through the stiffened web-flange junction path and redistributed toward the far end of the lid. However, these stresses are below yield and the plates remain elastic.

The total accumulated plastic strain in the liners and reinforcements are recorded in Figure 30. It again demonstrates that permanent damage is localized in the vicinity of contact with the maximum at the corner tip of the outer liner as it should be.

The effective stress in the concrete at 0.002, 0.004 and 0.006 second are plotted sequentially in Figures 31, 32 and 33 respectively. Stress localization at the contact region with the maximum at the corner tip reveals the response in the concrete being similar to that in the steel. The Stress wave propagation is clearly demonstrated by comparing Figure 32 against Figure 31. It identifies the growth of stress in the region and the transmitting of stress to the lid concrete through its contact with the inner face of the container. Comparing Figure 33 to Figure 32; the decrease of stress is very pronounced and is because of unloading due to the CIC rebound. It is interesting to note the difference in displacement between the inner face of the container and the lid. A slippage at the interface is apparent. This is because that the downward movement of the container itself has been stopped due to contact with the target pad, whereas, the lid continue to move downward not only due to its own weight but that of the payload as well.

The accumulated equivalent plastic strain in concrete is illustrated in Figure 34. The local contact region in color represents the portion of concrete being crushed. It is interesting to note that the concrete in the lid is not damaged at all.

Figure 35 is a stress distribution plot of the hydrostatic pressure in concrete at the peak load of 0.004 second. It indicates that the local region under direct impact subjects to direct compression (i.e., pressure).

6.2 1/8 Scale Model

Figures 36 shows the kinetic energy-time history of the 1/8 scale model during the course of impact. The figure identifies a full stop of the model at approximately 0.00265 second and a rebound thereafter. The smoothness of the curve again implies a stable numerical analysis. The contact force-time history between the model and the target pad is plotted in Figure 37 which indicates that a peak force of about 5.9×10^5 Newtons is reached at approximately 0.002 second.

Figures 38 and 39 display the deformed liners/reinforcements and the lid cover plate of the CIC respectively. The deformed shape, the localized damage at the contact area and the limited warping at the tip of the lid are all identical to that in the 1/4 scale model and have been discussed previously.

For the stress and strain, results are presented in the format identical to that of the 1/4 scale model. Figures 40 and 41 are the effective stress at the two extreme faces of the outer liner while Figure 42 provides the effective stress at the inner liner. Stress at the outer and inner layer of reinforcement is demonstrated in Figures 43 and 44 respectively.

Figures 45 and 46 show stress in the liners and reinforcements at 0.002 and 0.003 second. Figure 47 illustrates the stress in the lid cover plate. The accumulated plastic strain in the liners and reinforcement is presented in Figure 48. Figures 49 and 50 provide effective stress in the concrete at 0.002 and 0.003 second. The equivalent plastic strain accumulated in the concrete is shown in Figure 51, and finally the concrete hydrostatic pressure is plotted in Figure 52.

All these figures indicate that the 1/8 scale model responds identically to that of the 1/4 scale model. Observations have therefore been discussed previously and are omitted here.

7.0 COMPARISON BETWEEN 1/4 AND 1/8 SCALE MODELS

The analytical prediction of the response of the 1/4 and 1/8 scale models are compared using two approaches, 1) compare the individual corresponding plots and figures through visual examination and 2) compare the various items in accordance with the law of scale. These items are summarized in Table 2 with the correct scale ratios provided for direct comparison.

Comparing the kinetic energy and contact force (i.e., Figure 17 vs Figure 36, Figure 18 vs Figure 37), it can be found that the system responses of the two models are very consistent. This is demonstrated by the amount of initial kinetic energy, the time for the CIC to reach its full stop (i.e., kinetic energy drops to zero), the peak contact force, the time to reach peak contact force and the time when the CIC fully disengages from the target pad resulting in the contact force being dropping to zero (see Table 2).

Comparison of the deformations in the container (Figure 20 vs Figure 38) and the lid (Figure 21 vs Figure 39) are also very favourable. The shape of the deformation in the two models are identical even though the absolute magnitudes are different.

The stress and strain generated in the CIC should be identical regardless of scale size. By examining and comparing the contour plots of effective stress, plastic strain and hydrostatic pressure between the 1/4 and 1/8 scale models (i.e., Figures 22 through 35 vs Figures 40 through 52), it is seen that the stress/strain distributions are indeed identical. It should be noted that, due to the time ratio of two to one, the stress/strain at 0.004 second in 1/4 scale model is compared with that at 0.002 second in the 1/8 scale model and 0.006 second with 0.003 second etc. Also the peak stresses and strains are summarized in Table 2. They follow the one to one ratio very well. The slight difference could be either due to localized plasticity (material non-linearity) or simply due to numerical approximation in the computation. In any case the difference is very small and can be ignored.

8.0 COMPARISON BETWEEN ANALYTICAL AND EXPERIMENTAL RESULTS

Two items that can be compared directly between the analytical and experimental results are the acceleration and the physical deformation. They are discussed in the following:

8.1 1/4 Scale Model

Figures 53, 54 and 55 illustrate the acceleration time history predicted at the mid-height of the outer liner at three different positions, ninety (90) degree apart. The actual positions are identified in each individual figure. All three figures demonstrated a peak acceleration of approximately 500 g with a time period of about 0.006 second.

Figure 56 presents two recorded accelerometer readings (recorded as deceleration) at the mid-height of the outer liner and at the position shown. Theoretically, these two time histories should be identical due to symmetry even though this may not be practically possible. However, the two do show a consistent variation pattern and similar magnitudes.

Comparing Figures 54 and 56 for the material point at the same height and same position, the predicted peak magnitude of 500 g is very well matched to the recorded 501.4 g. The time period of 0.006 second to reach zero acceleration after a complete half cycle, as shown in Figure 54, also agrees with the recorded data (see Figure 56).

After the experimental drop, the model was cut at the most critically damaged area as shown in Figure 57a. It is noted that the cut passed right through the outer layer of vertical reinforcement and hence exposes its deformation shape. This shape of deformation is predicted very well by the analysis as demonstrated in Figure 25.

In Figure 57b, the solid line represents the outline of the damaged physical model from Figure 57a while the dotted line represents the analytical prediction. It can be seen that the deformation shape and magnitude have very good agreement except that the analytical prediction shifts consistently toward one side of the test results. This shift may be because the physical model did not hit the target pad at exactly the same orientation as that of the analysis.

8.2 1/8 Scale Model

Comparison of the 1/8 scale model follows the same pattern as that described in the 1/4 scale case.

Again Figures 58, 59 and 60 illustrate the predicted acceleration time history at the mid-height of the outer liner. The peak acceleration of approximately 1000 g and the time period of about 0.003 second demonstrate the consistency of a two to one ratio with the 1/4 scale model.

However comparison with the peak acceleration from experimental data is less favorable than for the 1/4 scale model as the two recorded readings being 1309 g and 1615 g respectively (Figure 61). These higher than expected values could be due to instrumentation and calibration. Also the smaller scale model induces higher acceleration which are subsequently more difficult to match exactly as demonstrated by the difference between the two recorded values. On the other hand, it should be noted that the time period of 0.003 second agrees with the experiment very well.

Figure 62a shows the cut specimen and Figure 62b demonstrates the direct comparison between analysis and test. Similarity to the 1/4 scale case is observed here on the consistent deformation shape and magnitude with a slight shift due to a minor deviation of impact orientation.

9.0 CONCLUSIONS

Two analyses to simulate 1/4 and 1/8 scale CIC model drop tests have been performed. The continuity and smoothness of the kinetic energy time history curve in both cases indicate that the two analyses are carried out successfully without experiencing any numerical instability. Results in terms of energy, contact force, deformation, stress and strain are examined in detail and comparison are made between the two models as well as against experimental results.

On the impact response of the CIC, higher stress and strain are concentrated in the vicinity of contact and quickly reduced to lower levels toward remote areas. Permanent damage is therefore limited to the impacting corner. The stress/strain distribution and the deformation shape appear macroscopically very reasonable and is consistent with engineering intuition and the principles of physics.

When comparing the analytical results between the two models, either qualitatively in terms of stress/strain distribution patterns, or quantitatively in terms of peak values, the two cases match very consistently. When comparing the analytical predictions against test results in terms of acceleration and deformation, the agreement is also very favourable.

These two analyses provide evidence that the computer code DYNA3D is a reliable tool for impact analyses of the CIC, although the code should be used with caution due to its sophistication in the mathematical and computing treatment of the impact problem.

Approved by:

G.J. Clarke
Manager
Mechanical Research Department

Submitted by:

H.P. (Jack) Lee
Engineer
Applied Mechanics Section

Recommended by:

J.A. Chadha
Section Head
Applied Mechanics Section

Reviewed by:

T.P. Byrne
Unit Head-Stress Analysis & Heat Transfer
Applied Mechanics Section

REFERENCES:

1. J.D. Tulk, "Scalability of Concrete Containers under Impact Loads", Ontario Hydro Research Report No. 88-301-K, Jan 17, 1989.

2. R.G. Sauve, "Ontario Hydro DYNA3D Computer Code System VAX/VMS Version" Ontario Hydro Report No. 87-222, November 1987.

3. "Irradiated Fuel Storage Program, Concrete Integrated Cask, 1/4 Scale Model, Concrete & Steel Liner", Civil Design Department, Ontario Hydro Drawing No. 0973-D2H-03760-0014-Rev. 0, October 5, 1987.

4. "Irradiated Fuel Storage Program, Concrete Integrated Cask, 1/8 Scale Model, Concrete and Steel Liner", Civil Design Department, Ontario Hydro Drawing No. 0973-D2H-03760-0013-Rev. 0, October 5, 1987.

5. J.A. Sato, and H. Andre, "Concrete Integrated Container (CIC) Program, Construction of 1/4 and 1/8 Scale Models", Ontario Hydro Research Report No. 88-97-K, May 20, 1988.

6. "Irradiated Fuel Storage Program, Concrete Integrated Cask, 1/4 Scale Model, Reinforcing Details", Civil Design Department, Ontario Hydro Drawing No. 0973-D2H-03760-0014-Rev. 0, October 1987.

7. "Irradiated Fuel Storage Program, Concrete Integrated Cask, 1/8 Scale Model, Reinforcing Details, Civil Design Department, Ontario Hydro Drawing No. 0973-D2H-03760-0013-Rev. 0, October 1987.

TABLE 1

CONCRETE PROPERTIES

	First Cast		Second Cast	
	28-day	Day of Test	28-day	Day of Test
Compressive strength (MPa)	42.9	45.3	41.2	44.8
Split tensile strength (MPa)	-	4.3	3.8	4.0
Modulus of Elasticity (MPa)	46,340	46,920	45,785	45,800
Density (kg/m^3)	-	3,533	-	3,536

TABLE 2: COMPARISON BETWEEN 1/4 AND 1/8 SCALE MODELS

		1/4 SCALE MODEL	1/8 SCALE MODEL	RATIO
CIC SYSTEM	Initial Kinetic Energy (Total Energy)	5.34×10^4 J	6.65×10^3 J	8:1
	Time to Reach Full Stop	0.0052 second	0.00265 second	2:1
	Peak Contact Force	23.8×10^5 N	5.9×10^5 N	4:1
	Time to Reach Peak Force	0.004 second	0.002 second	2:1
	Time to Disengage From Target Pad	0.00646 second	0.00323 second	2:1
STEEL LINERS & REINFORCEMENT	Peak Stress at Peak Load	1076/1035 MPa	1073/1030 MPa	1:1
	Peak Stress After Reloading	1038 MPa	1042 MPa	1:1
	Accumulated Plastic Strain	0.464	0.462	1:1
CONCRETE	Peak Stress at Peak Load	163 MPa	162 MPa	1:1
	Peak Stress After Reloading	94.3 MPa	98.5 MPa	1:1
	Accumulated Plastic Strain	0.457	0.445	1:1
	Peak Pressure	219 MPa	217 MPa	1:1

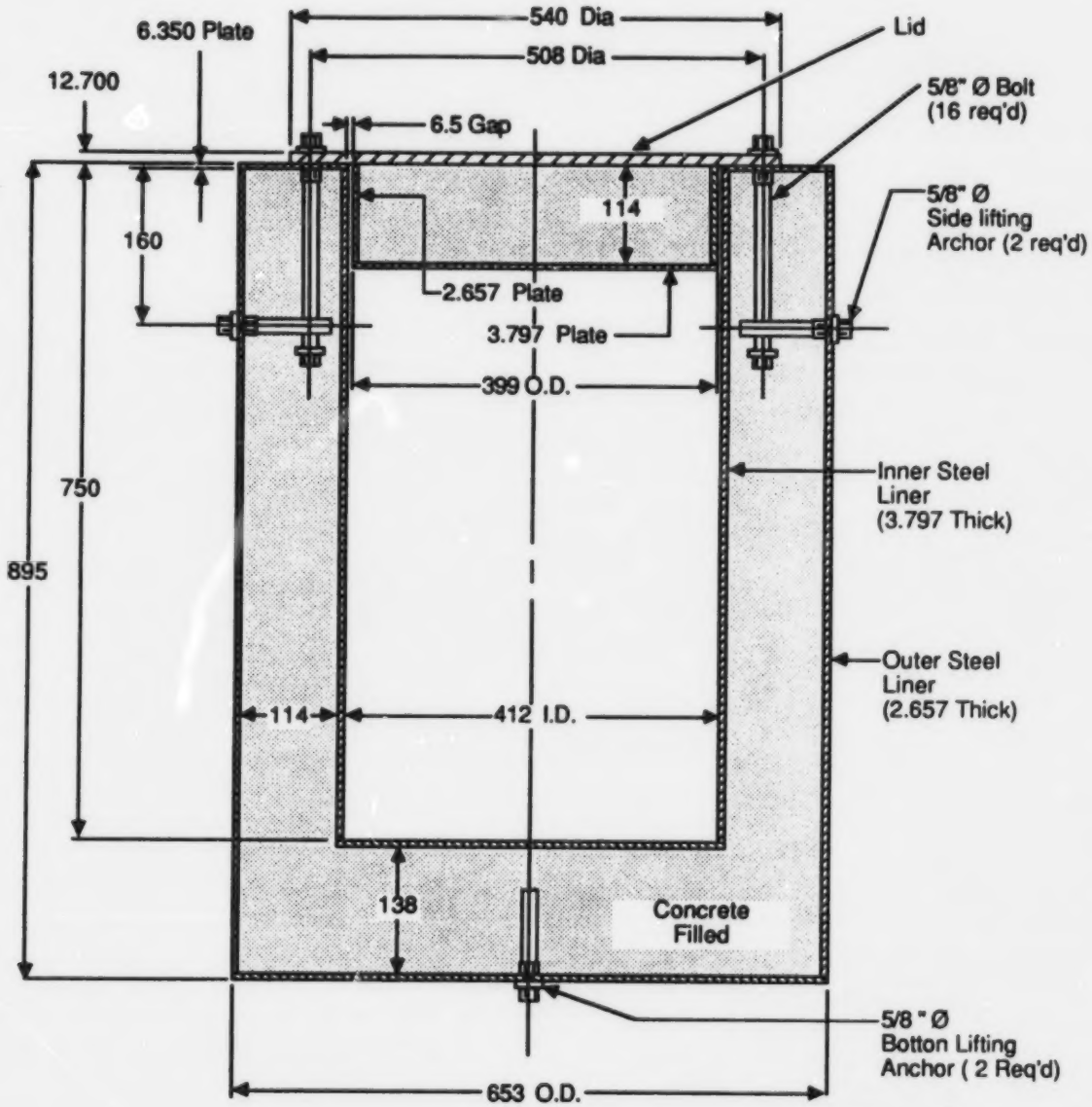

Notes:

1. All dimensions are in mm (unless otherwise noted)

FIGURE 1
1/4 SCALE MODEL DIMENSIONS

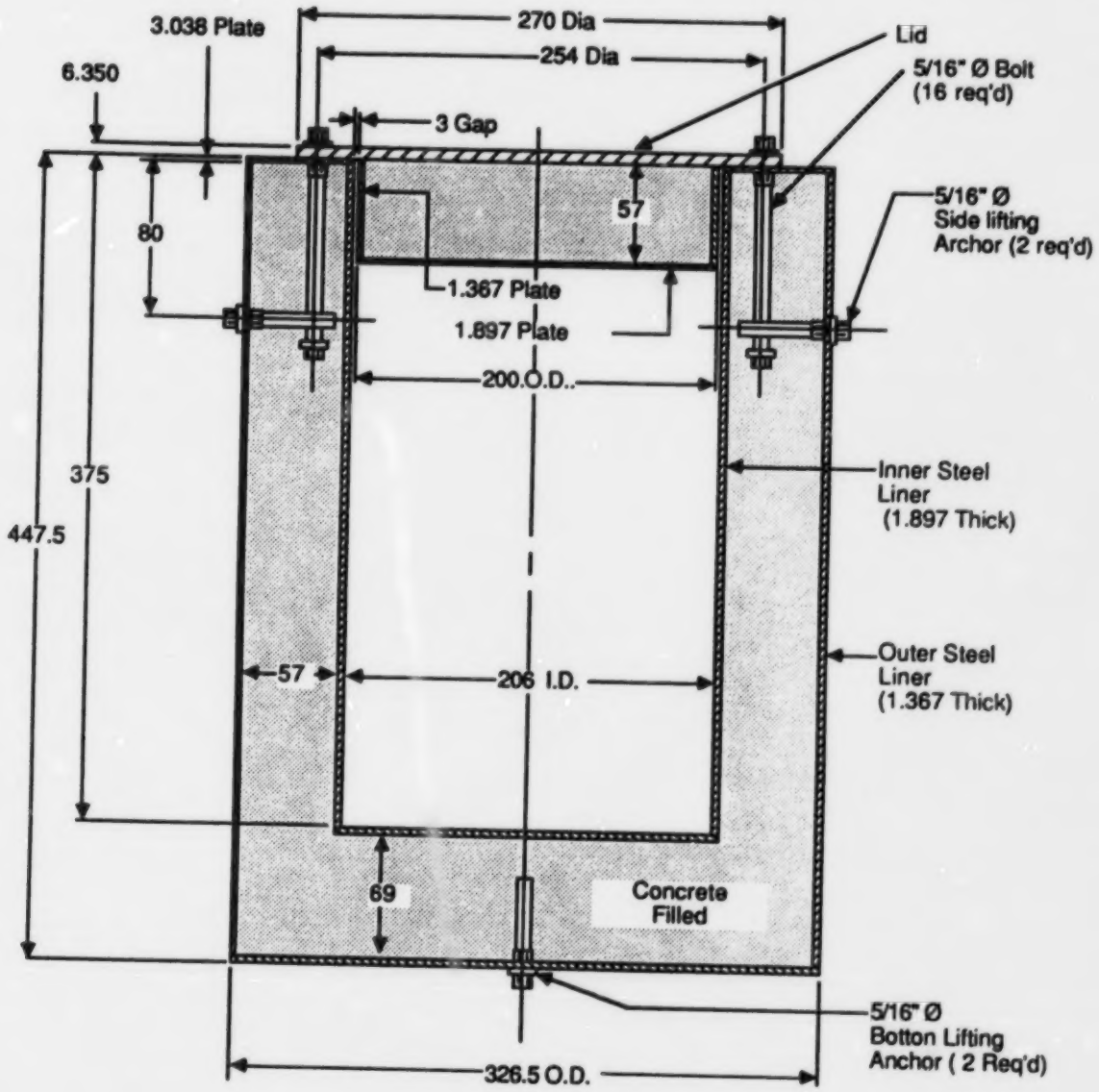

Notes:

1. All dimensions are in mm (unless otherwise noted)

FIGURE 2
1/8 SCALE MODEL DIMENSIONS

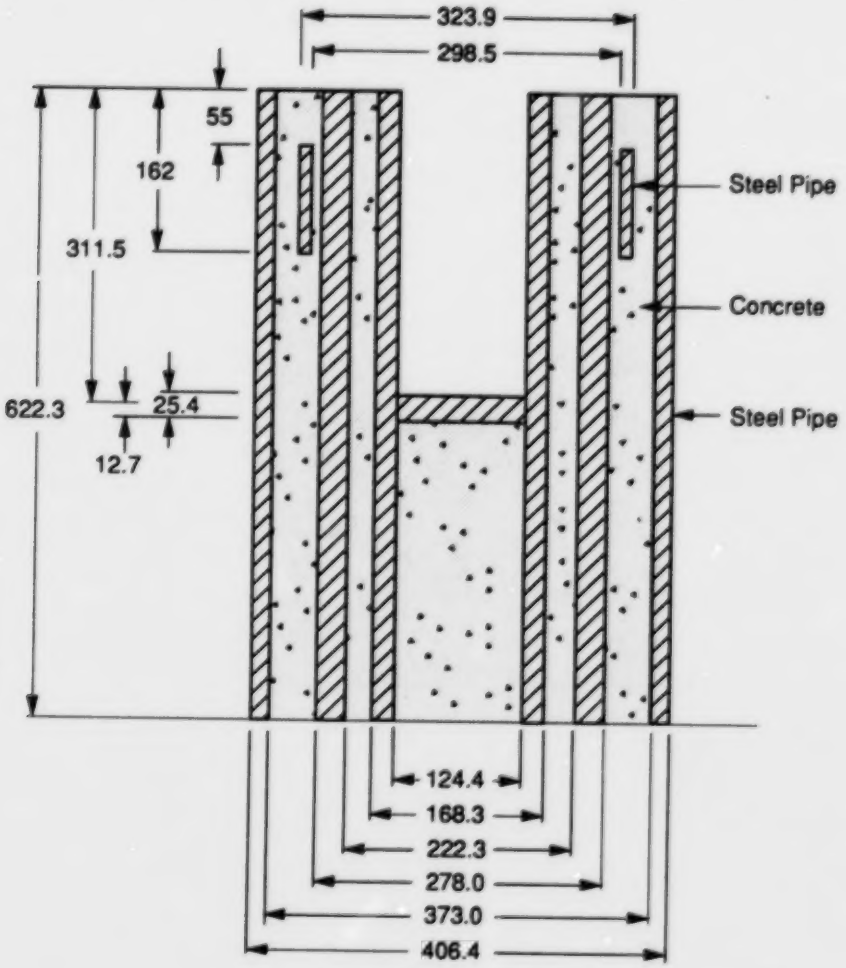

(a) SECTION VIEW

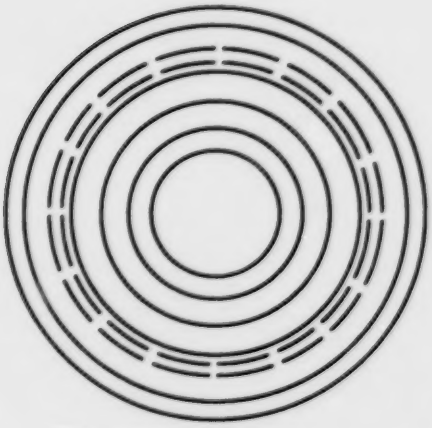

(b) PLANE VIEW

Note:

All dimensions are in mm

FIGURE 3

PAY-LOAD FOR THE 1/4 SCALE MODEL

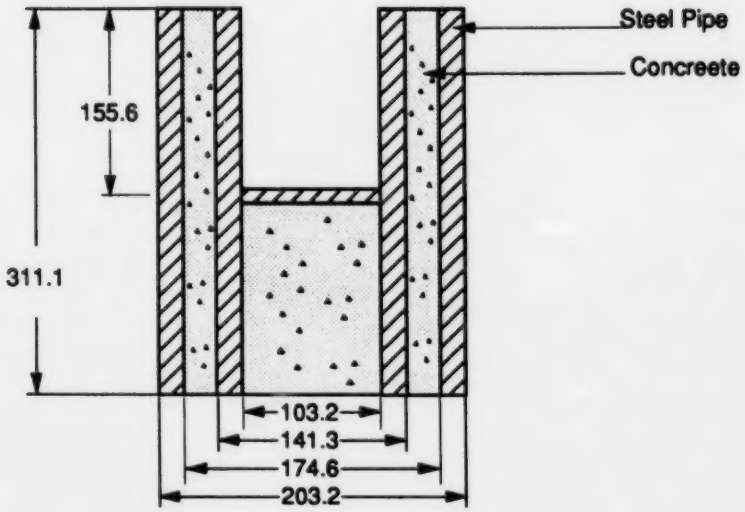

(b) SECTION VIEW

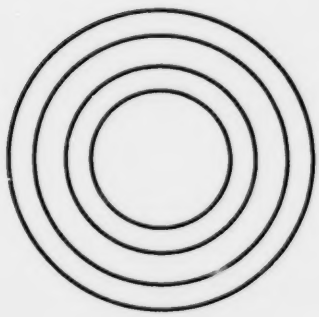

(b) PLANE VIEW

Note:

All dimensions are in mm

FIGURE 4

PAY LOAD FOR THE 1/8 SCALE MODEL

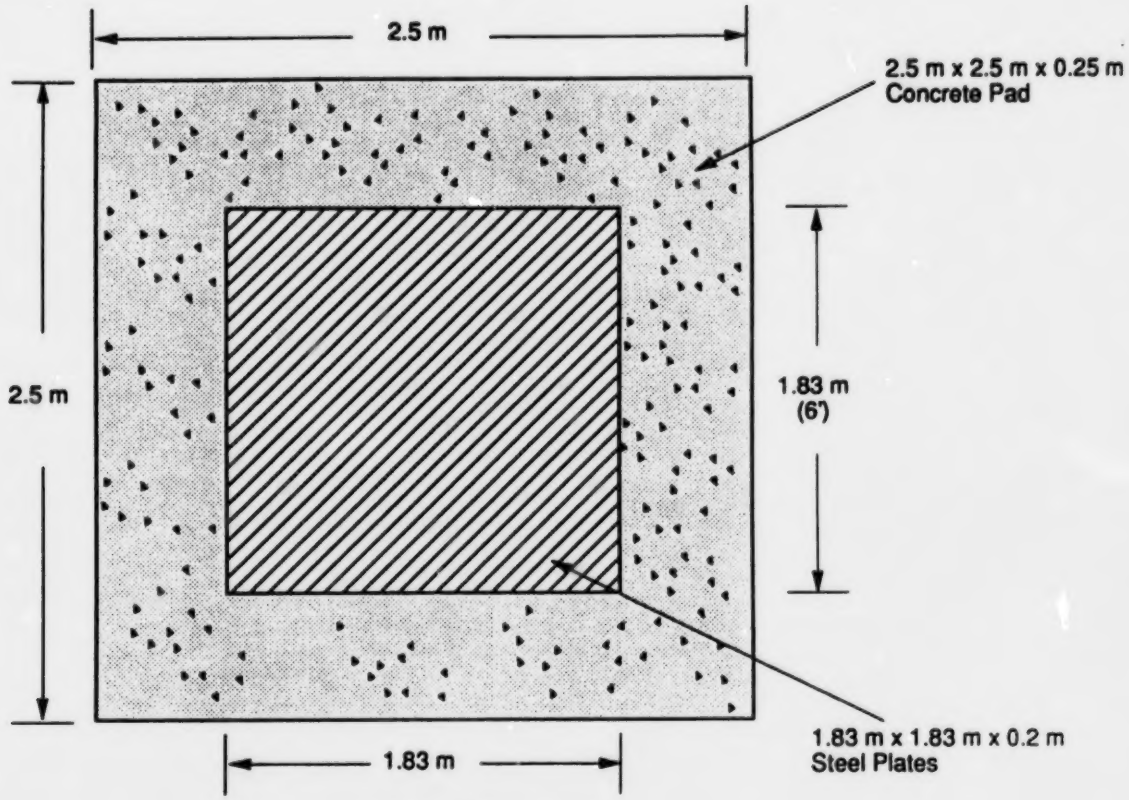

PLAN VIEW

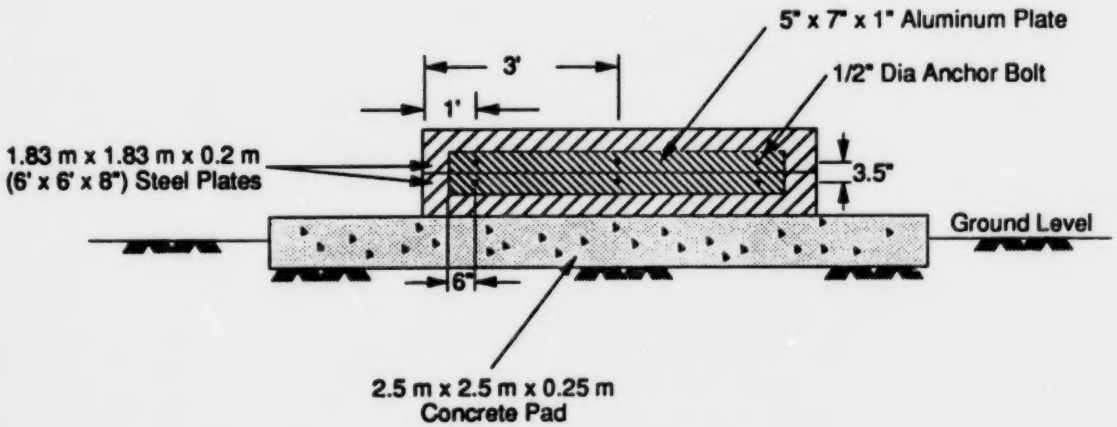

SECTION VIEW

FIGURE 5

TARGET PAD DIMENSIONS

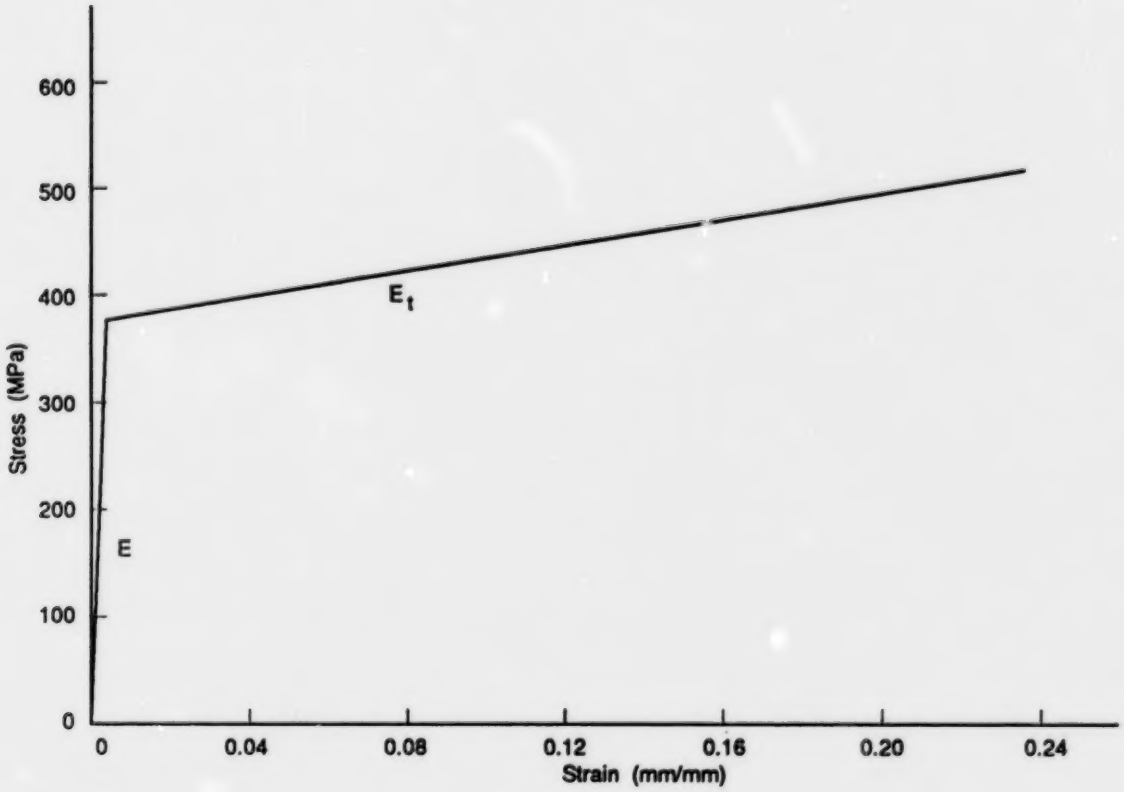

FIGURE 6

STRESS-STRAIN RELATION OF STEEL LINER

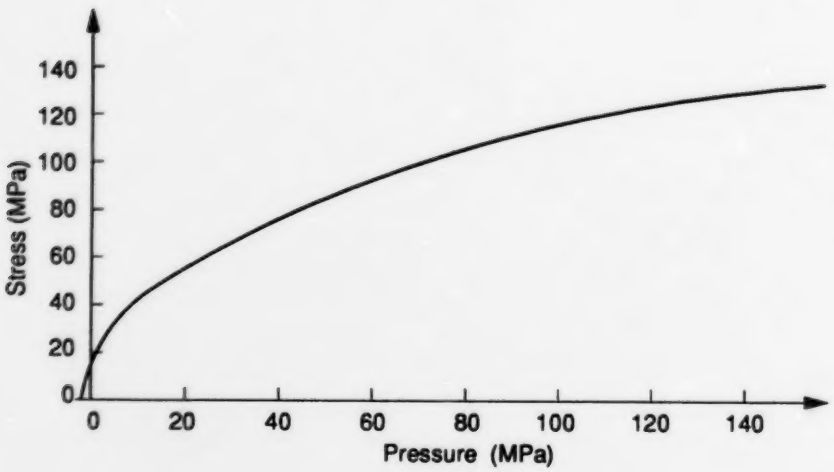

FIGURE 7

YIELD STRESS-PRESSURE RELATION OF CONCRETE

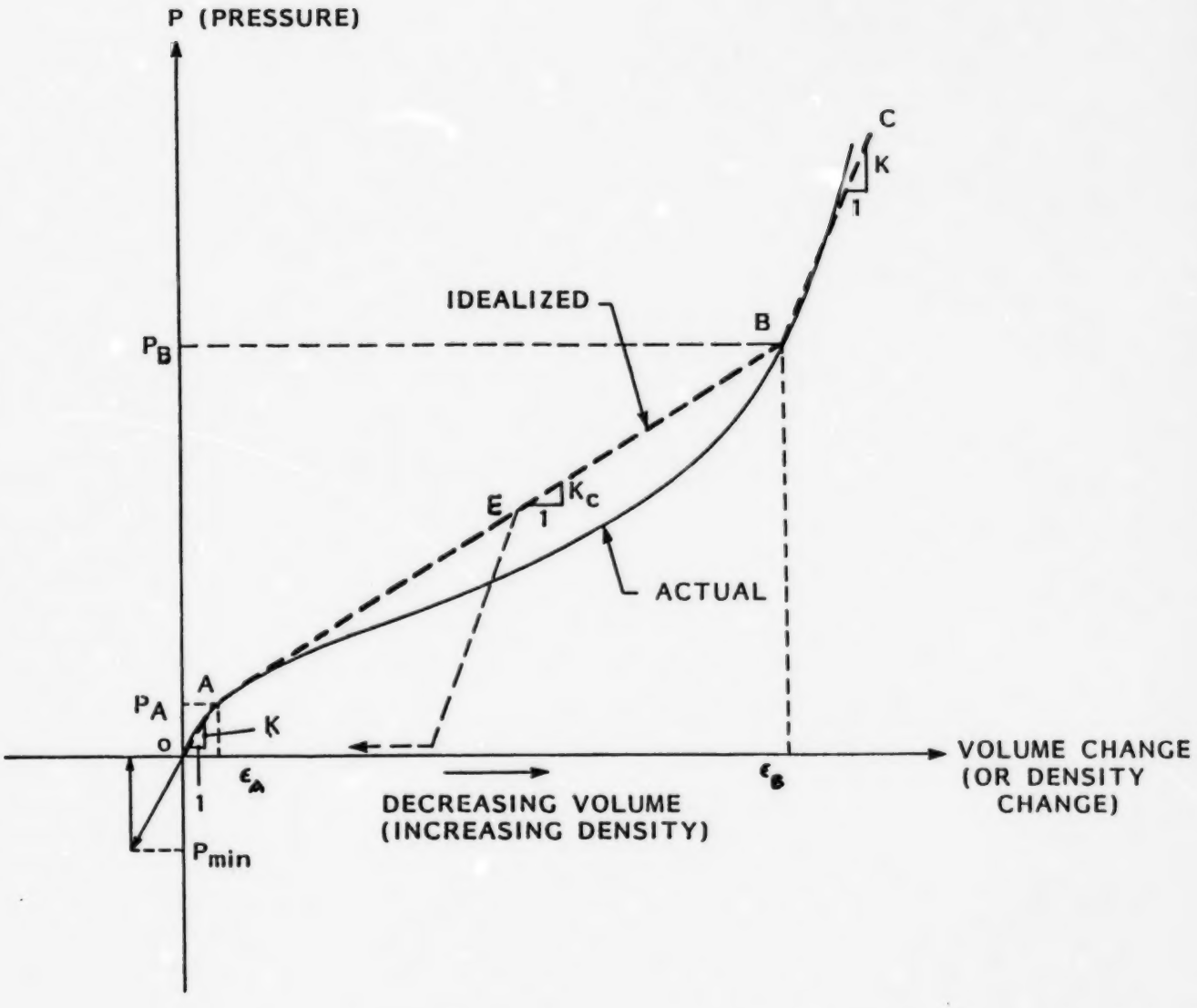

FIGURE 8

TYPICAL EQUATION OF STATE CURVE FOR GRANULAR MATERIALS

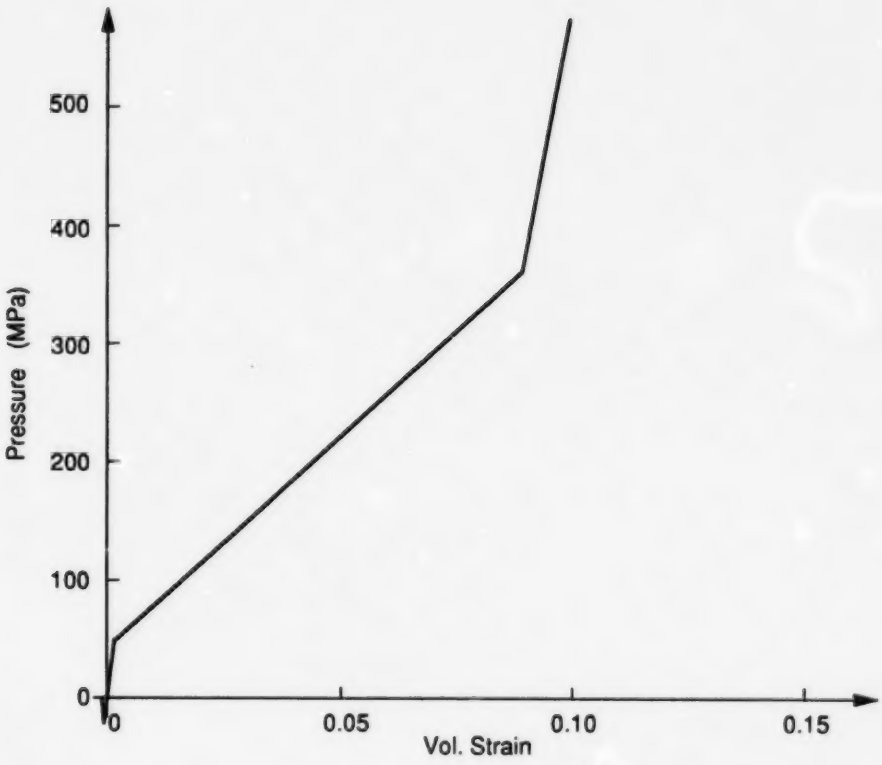

FIGURE 9

EQUATION OF STATE MODEL FOR CONCRETE

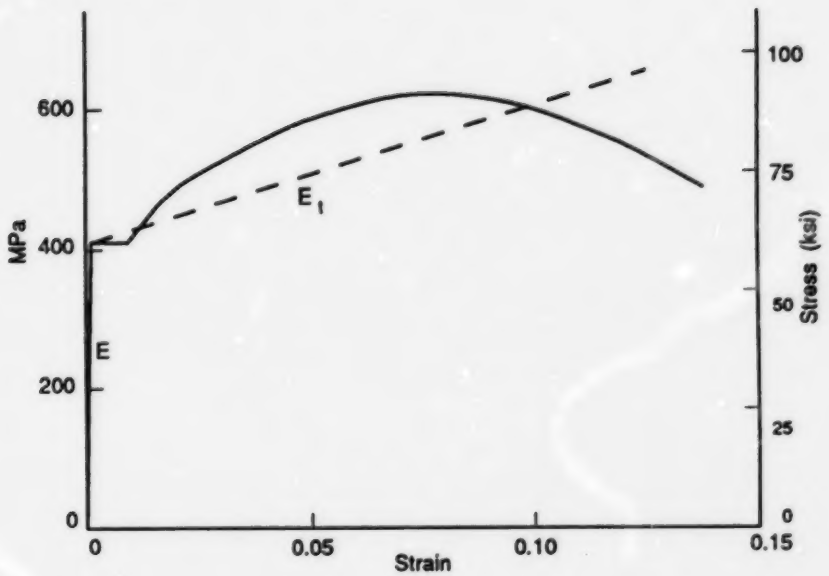

FIGURE 10

TYPICAL STRESS-STRAIN CURVE FOR GRADE 60 BILLET REINFFORCING STEEL

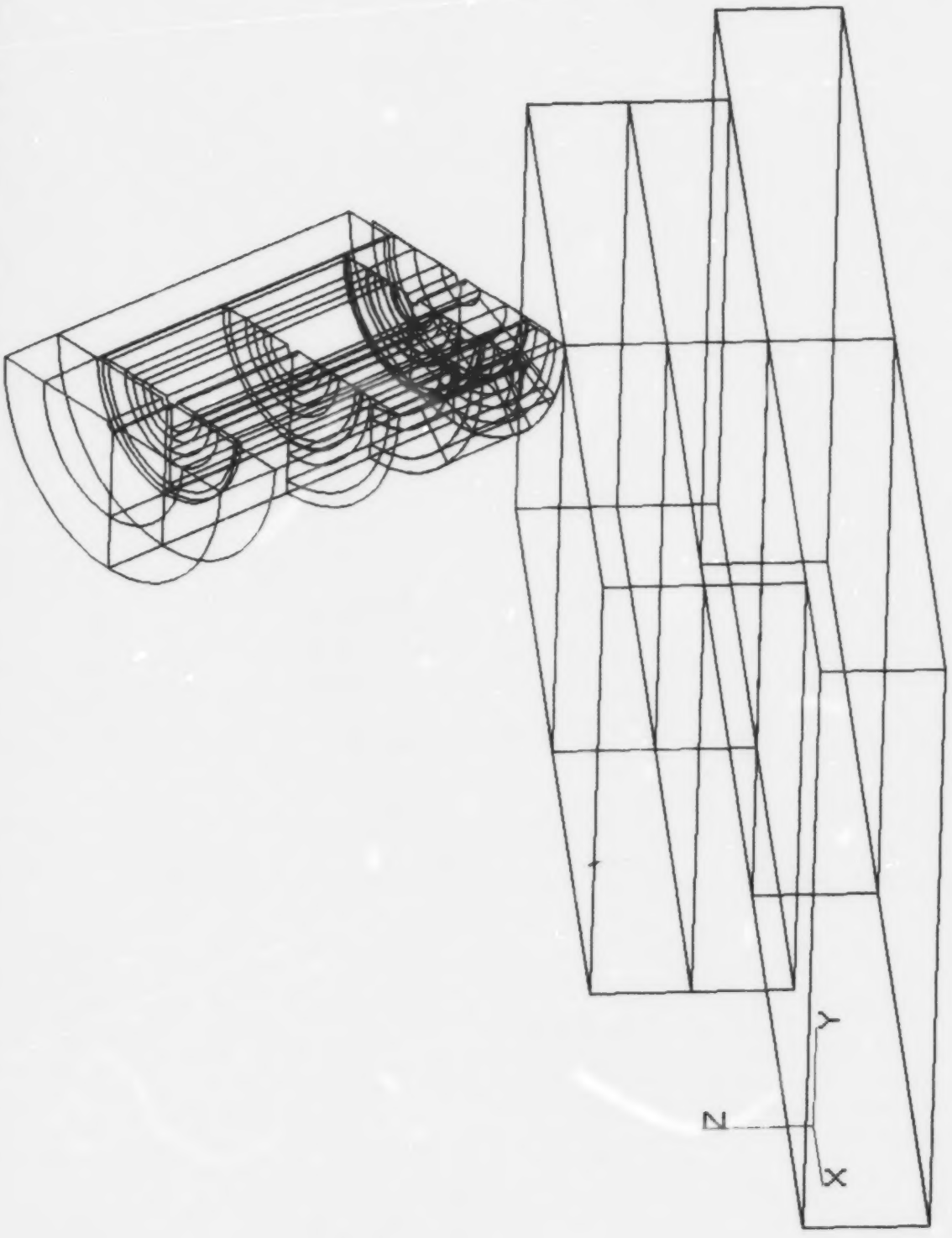

FIGURE 11
SKELETON OF THE CIC AND TARGET PAD
(1/4 SCALE MODEL)

89-298

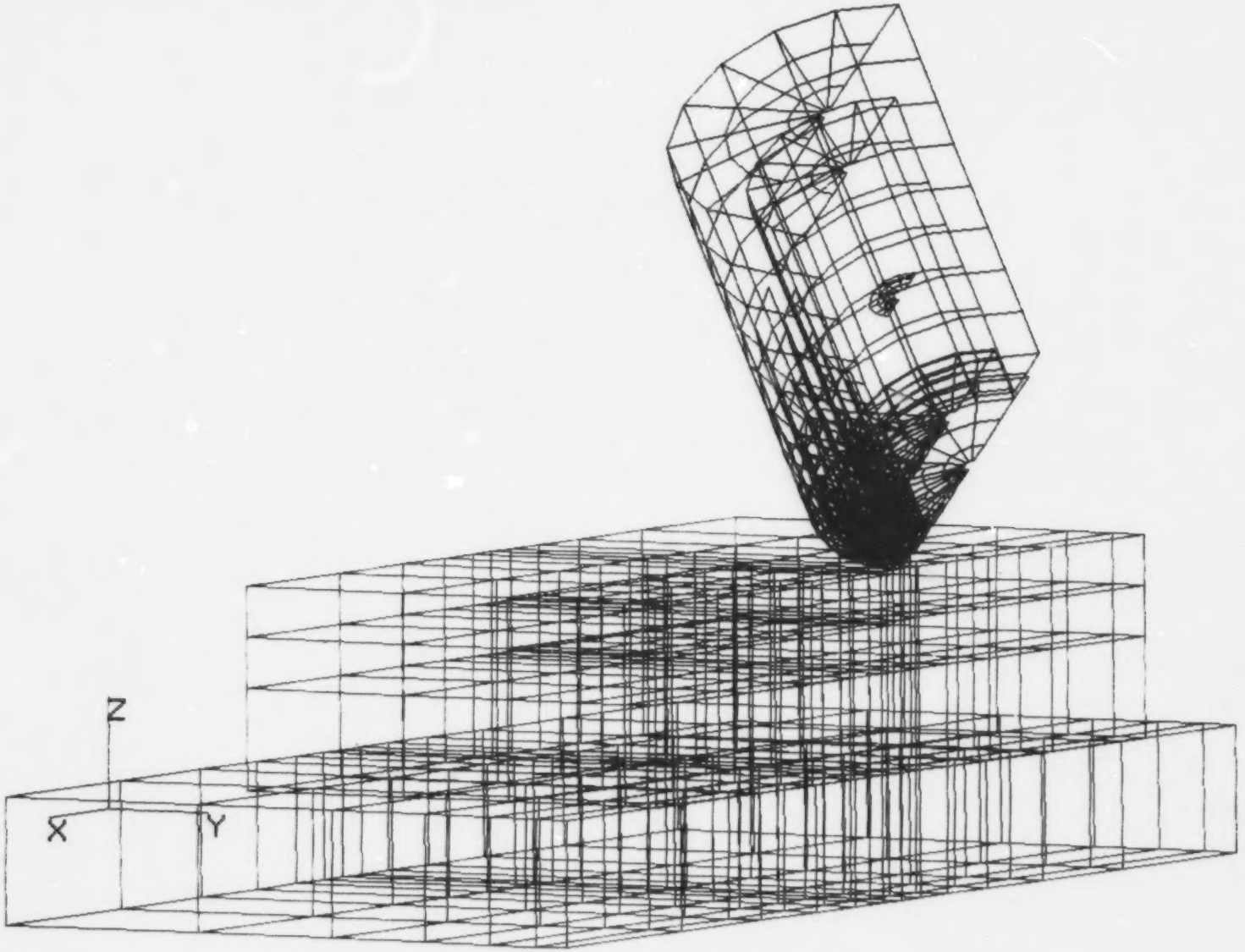

FIGURE 12

FINITE ELEMENT SIMULATION OF THE CIC STEEL LINERS AND TARGET PAD (1/4 SCALE MODEL)

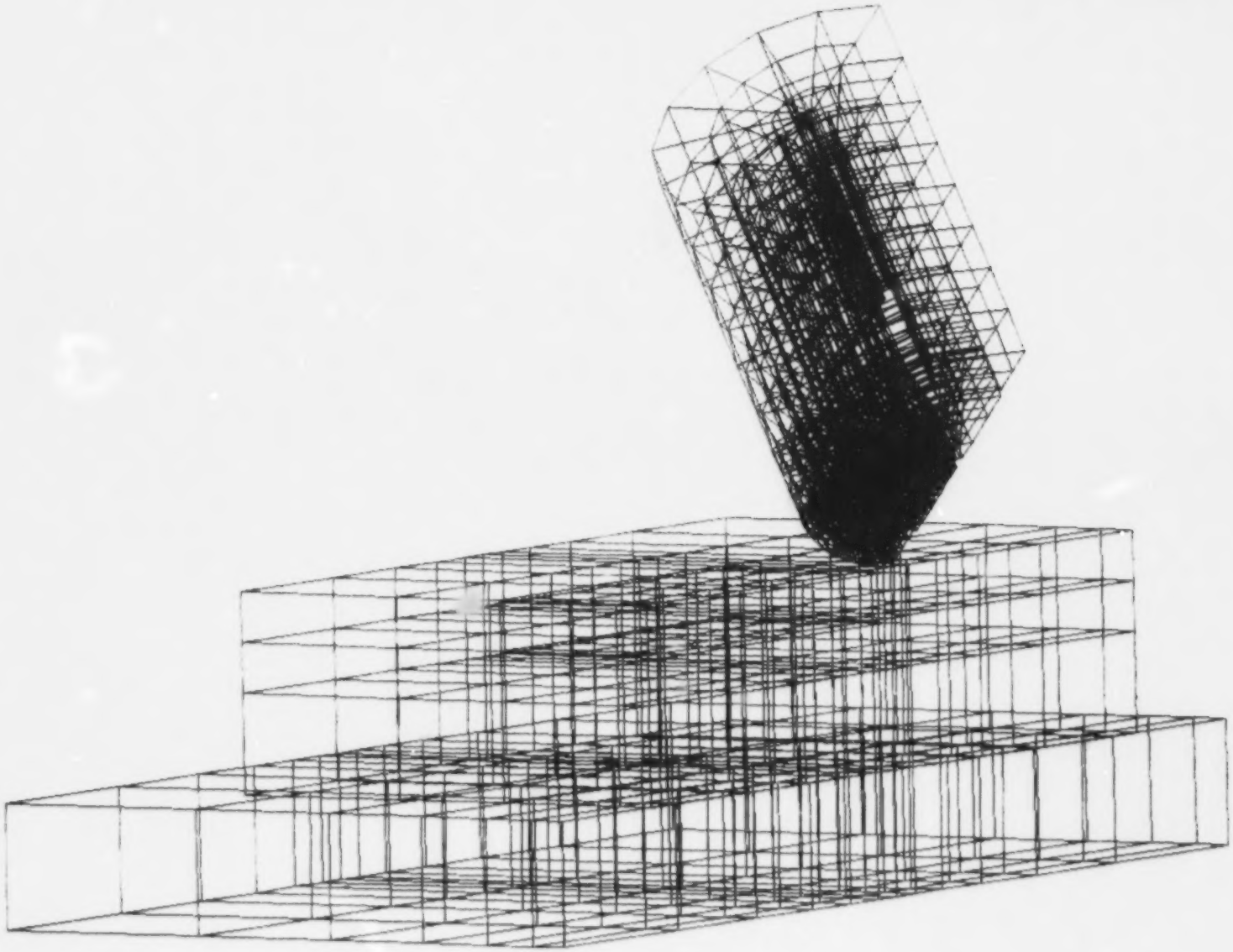

FIGURE 13

FINITE ELEMENT SIMULATION OF THE CIC CONCRETE, PAYLOAD AND TARGET PAD (1/4 SCALE MODEL)

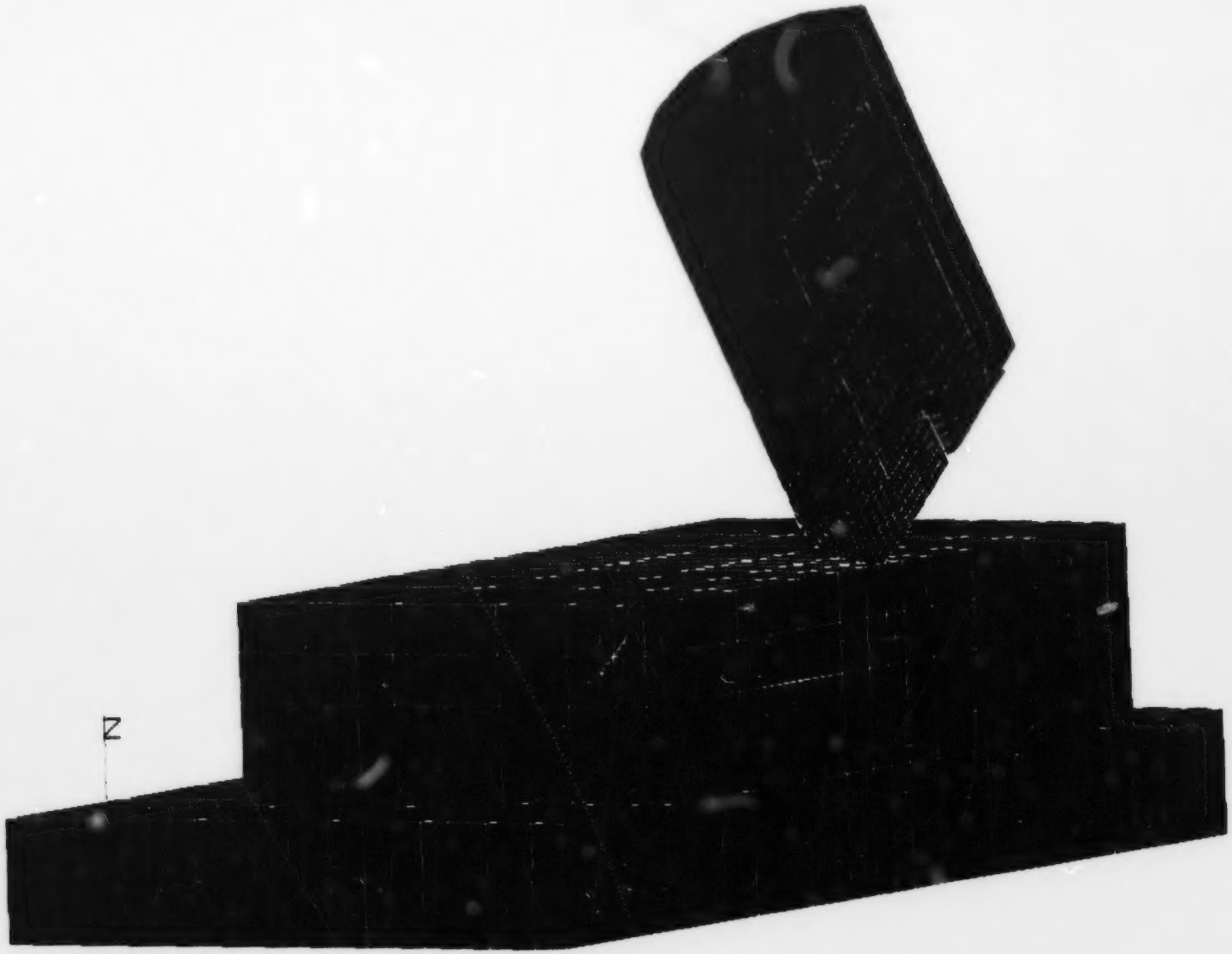

FIGURE 14

FINITE ELEMENT MODEL OF THE COMPLETE SYSTEM
(1/4 SCALE MODEL)

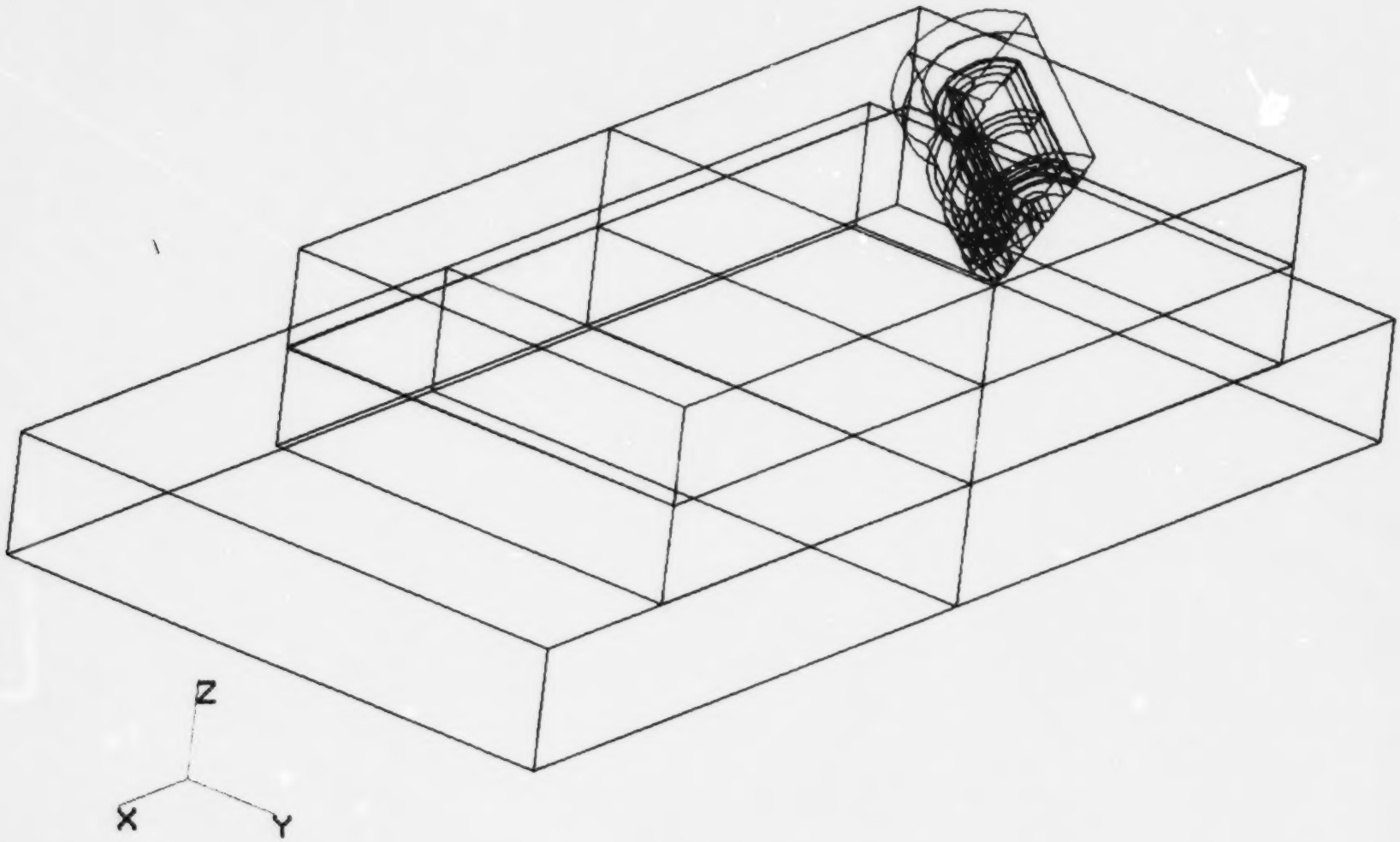

FIGURE 15

SKELETON OF THE CIC AND TARGET PAD
(1/8 SCALE MODEL)

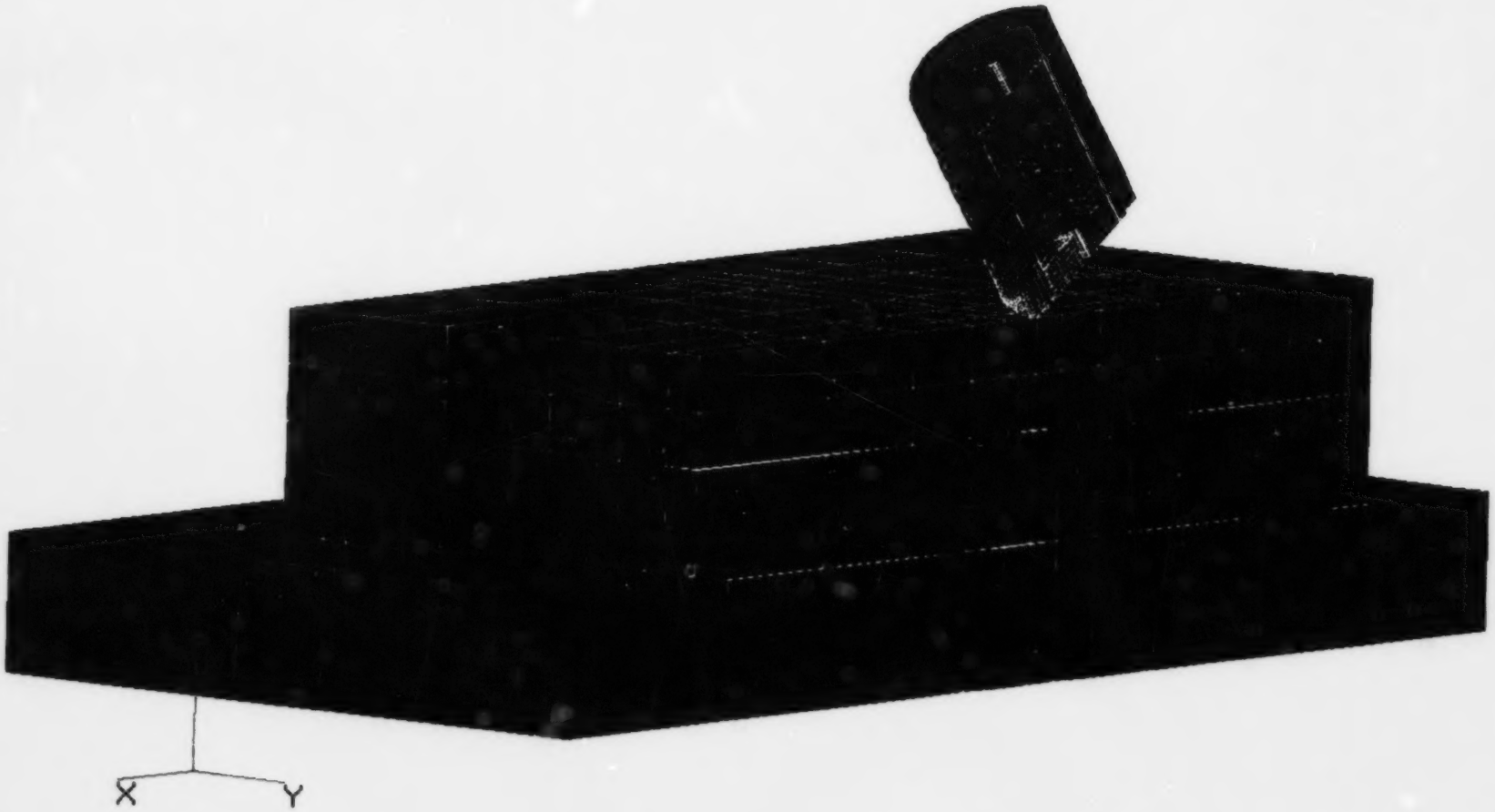

FIGURE 16

FINITE ELEMENT MODEL OF THE COMPLETE SYSTEM
(1/8 SCALE MODEL)

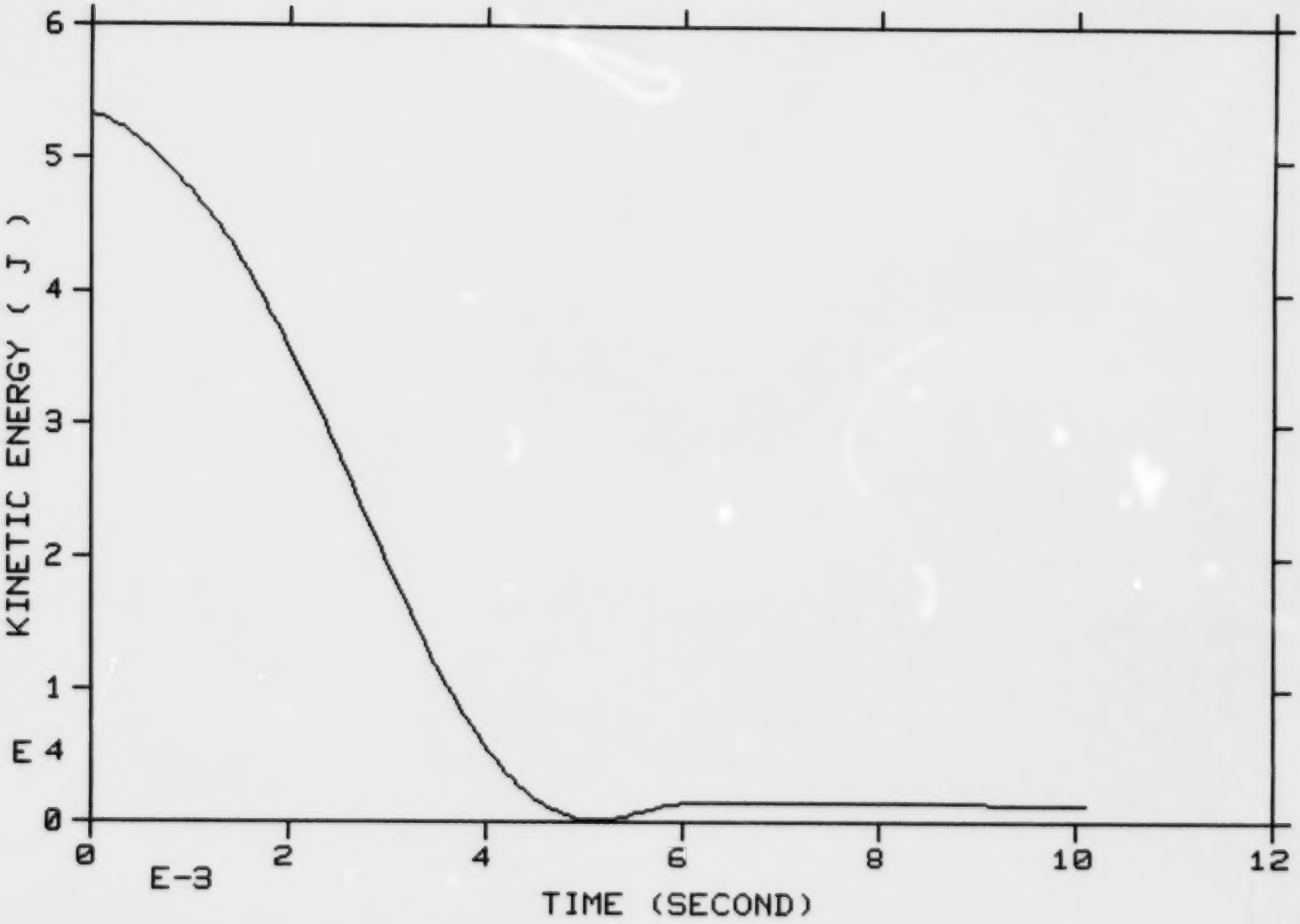

FIGURE 17

KINETIC ENERGY TIME HISTORY OF THE CIC
(1/4 SCALE MODEL)

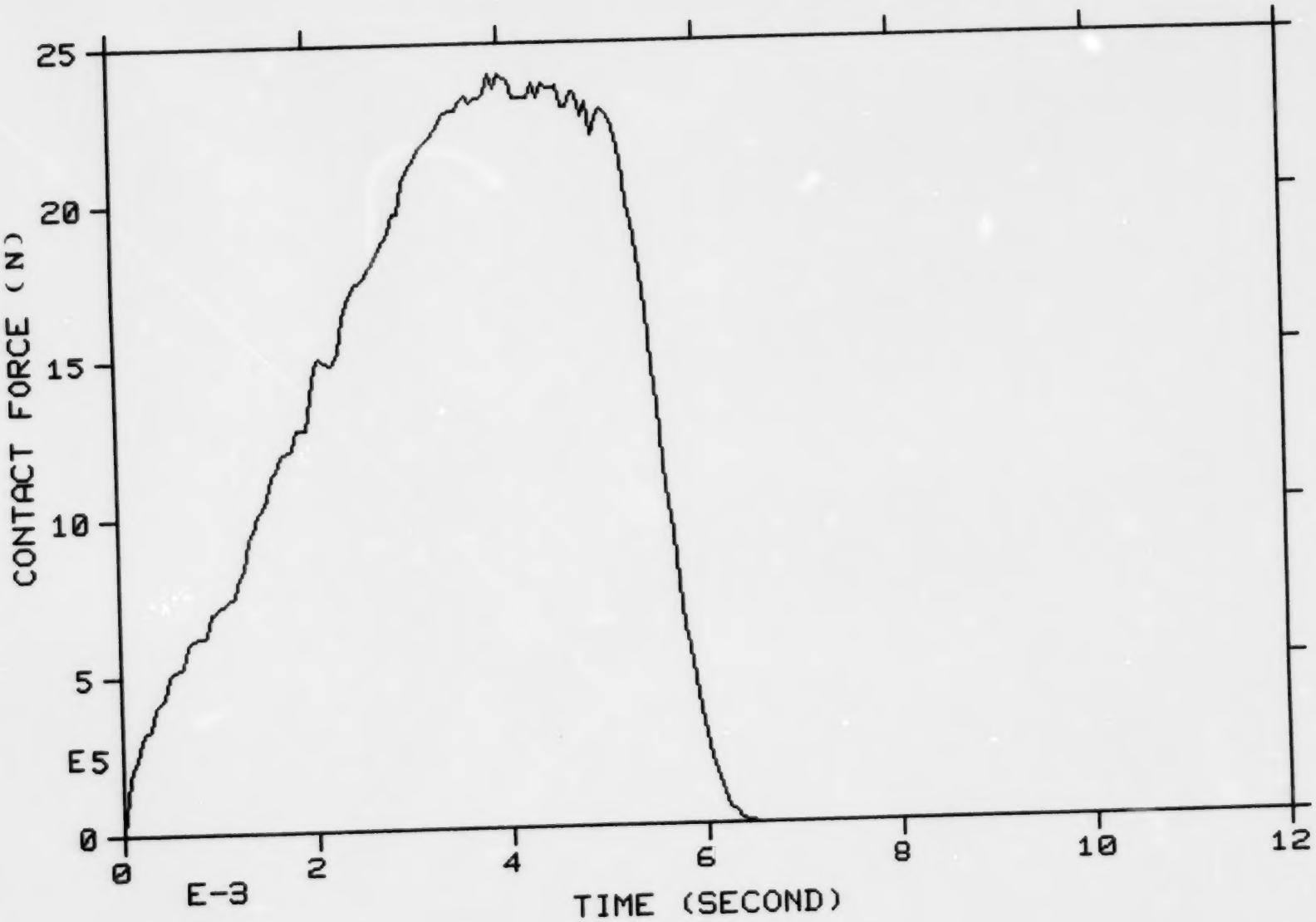

FIGURE 18

CONTACT FORCE TIME HISTORY OF THE CIC (1/4 SCALE MODEL)

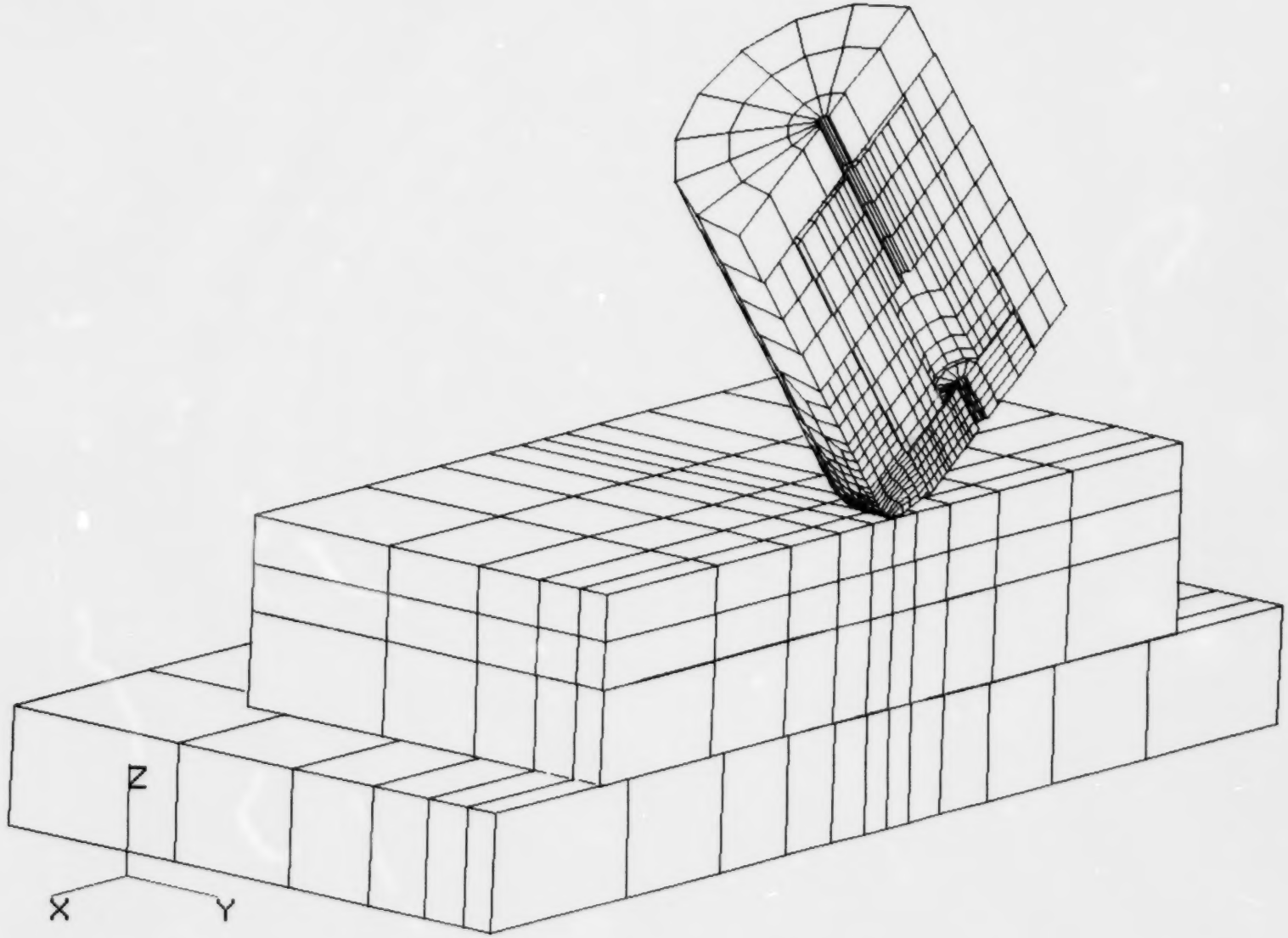

FIGURE 19

DEFORMATION OF THE CIC AT 0.01 SECOND (1/4 SCALE MODEL)

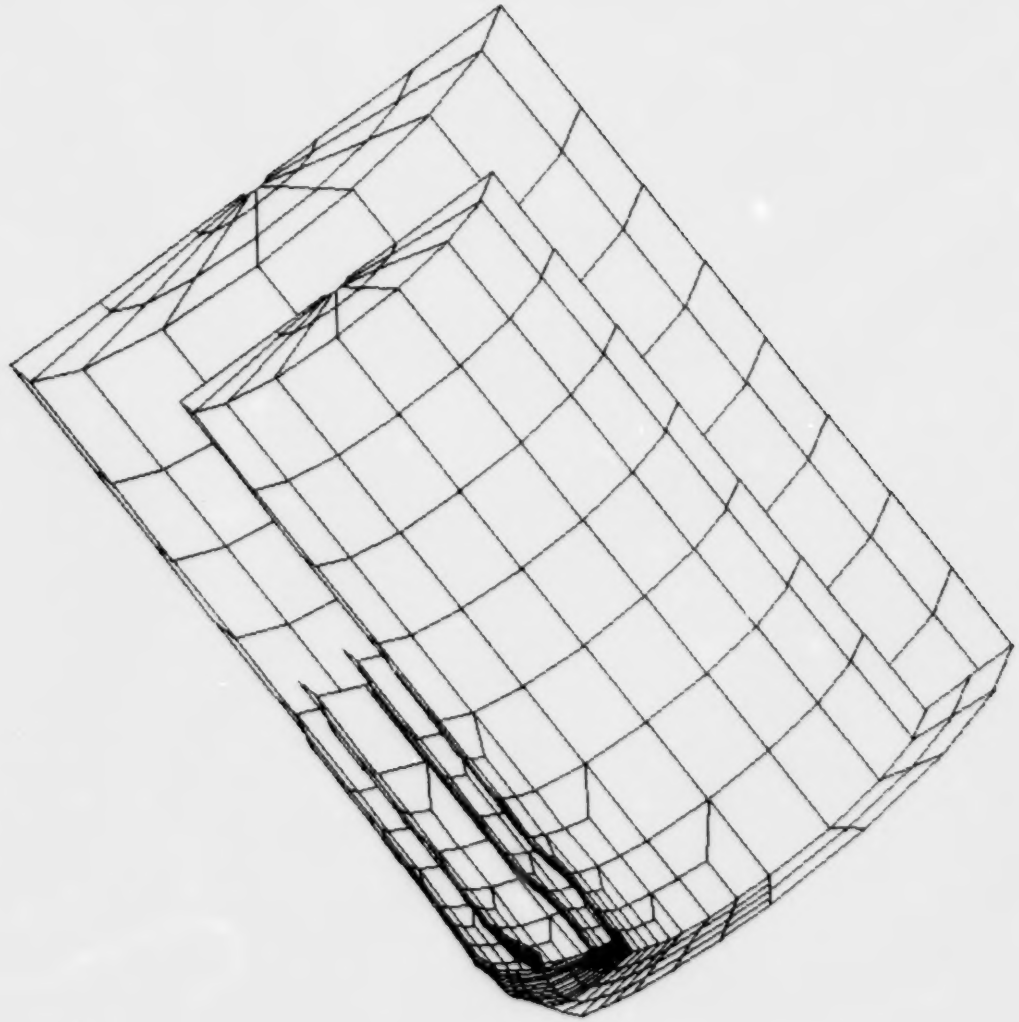

FIGURE 20

DEFORMATION OF THE STEEL LINERS AND REINFORCEMENTS AT 0.008 SECONDS (1/4 SCALE MODEL)

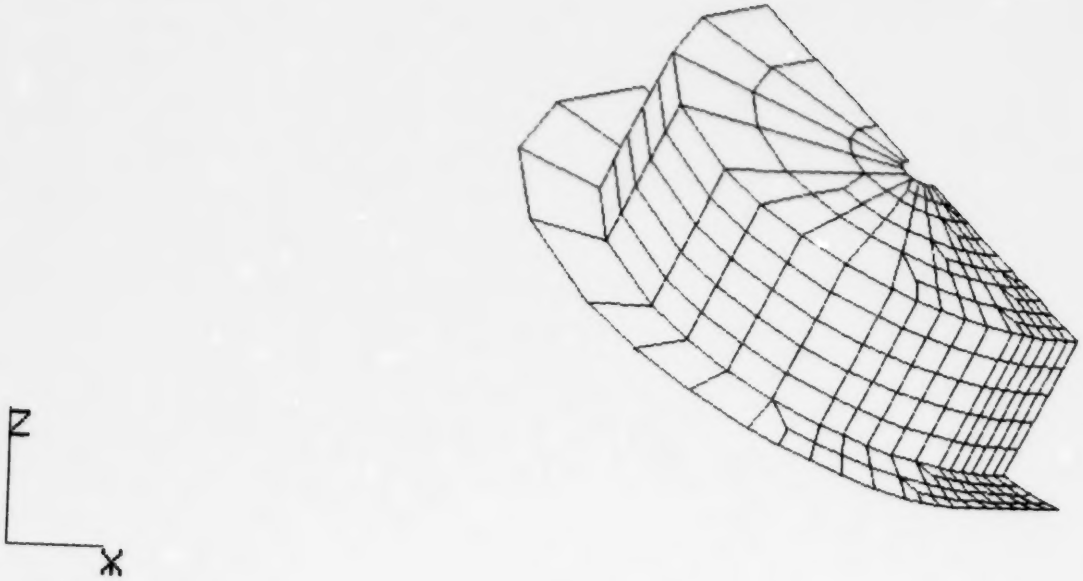

FIGURE 21

DEFORMATION OF THE STEEL LID PLATE AT 0.008 SECONDS (1/4 SCALE MODEL)

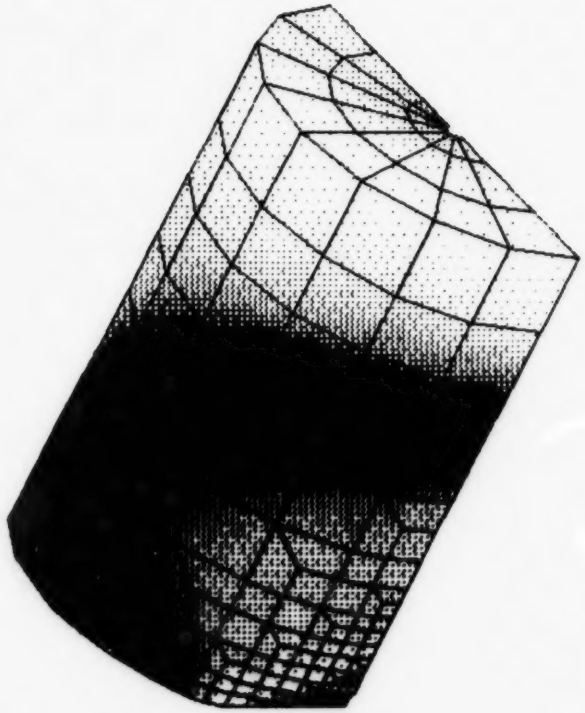

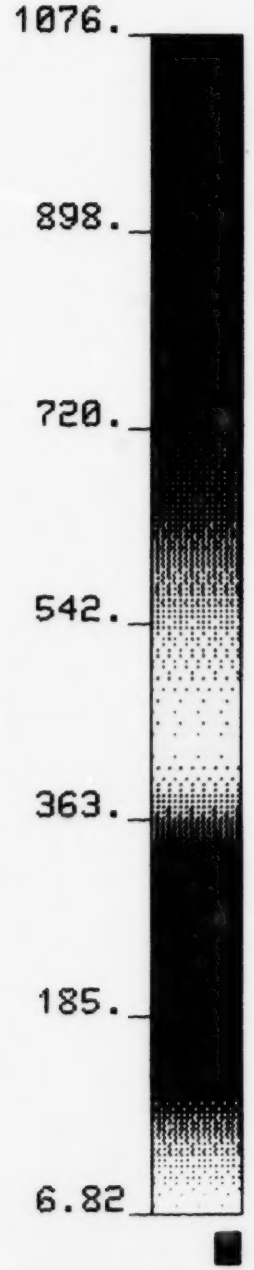

34

89-298

CIC 9M DROP
TIME= 0.004

FIGURE 22

VON MISES STRESS ON THE OUTSIDE FACE OF THE OUTER LINER AT 0.004 SECONDS (MPa) (1/4 SCALE MODEL)

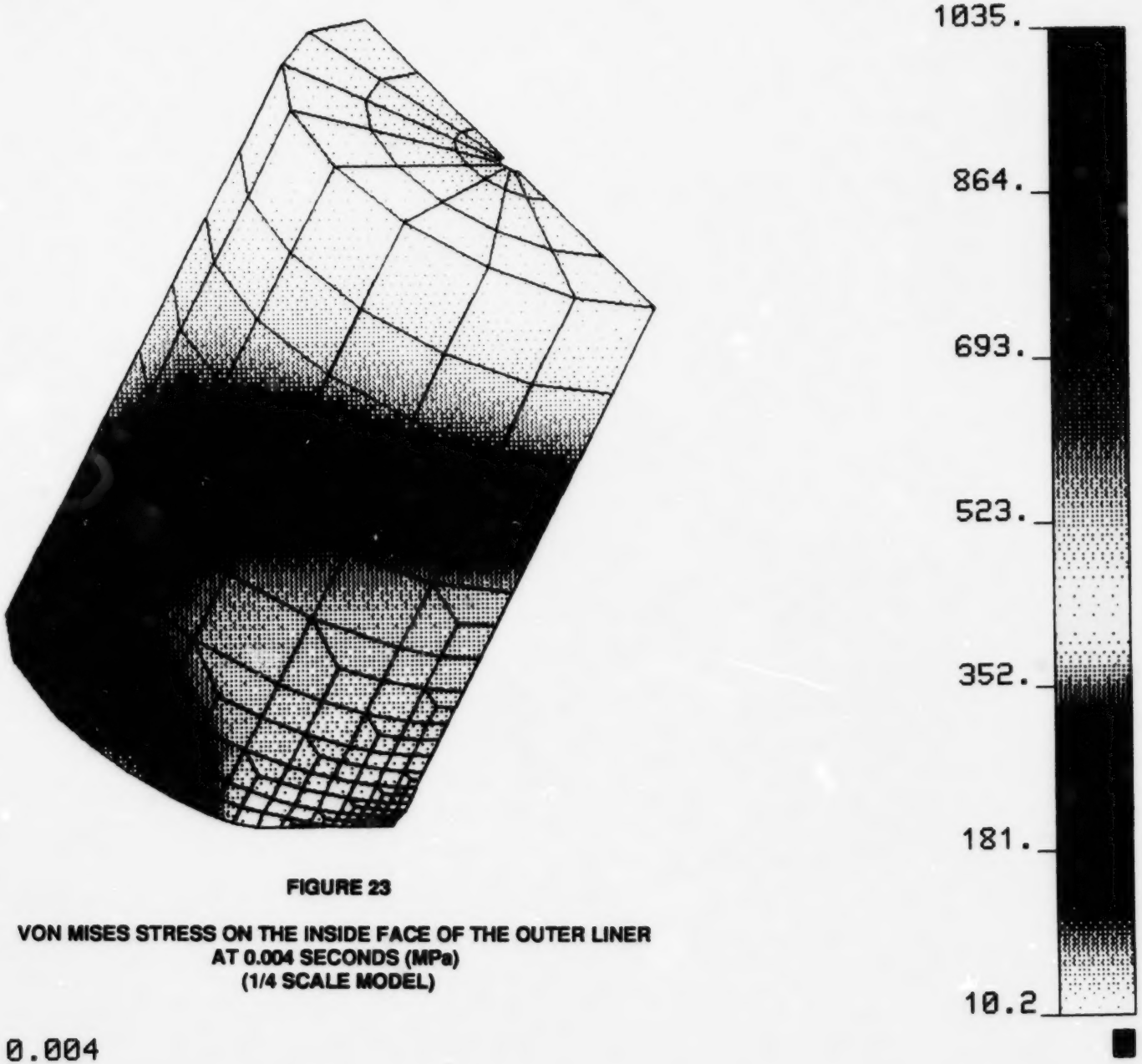

FIGURE 23

VON MISES STRESS ON THE INSIDE FACE OF THE OUTER LINER AT 0.004 SECONDS (MPa) (1/4 SCALE MODEL)

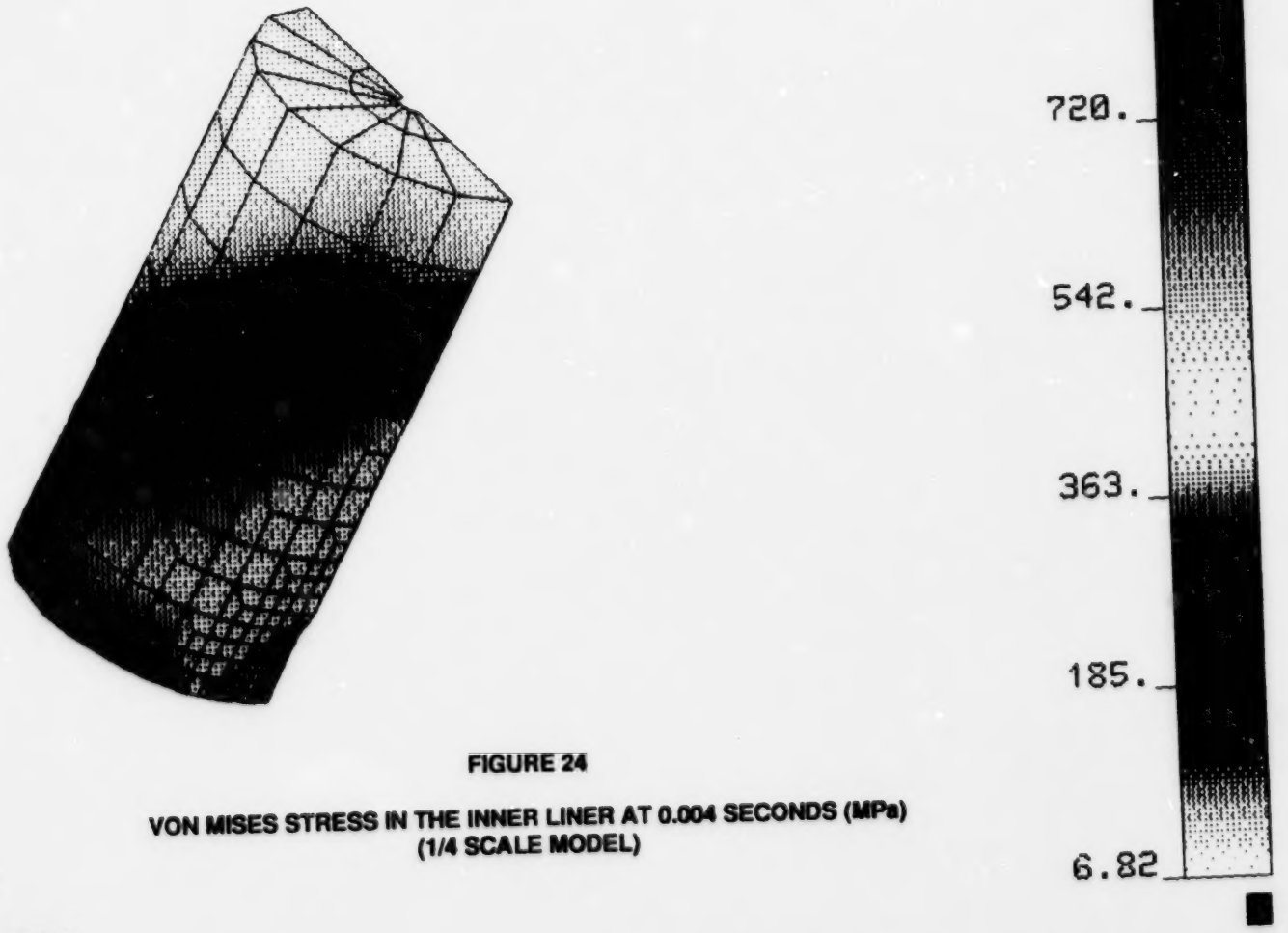

FIGURE 24

VON MISES STRESS IN THE INNER LINER AT 0.004 SECONDS (MPa)
(1/4 SCALE MODEL)

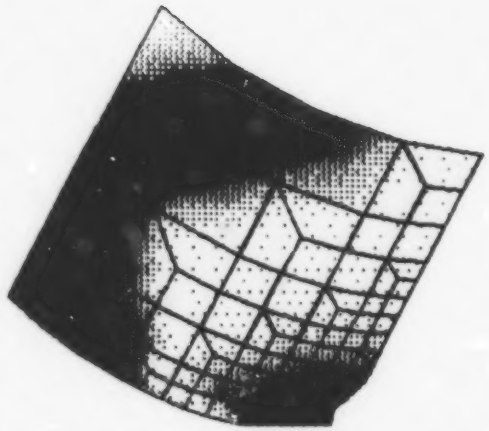

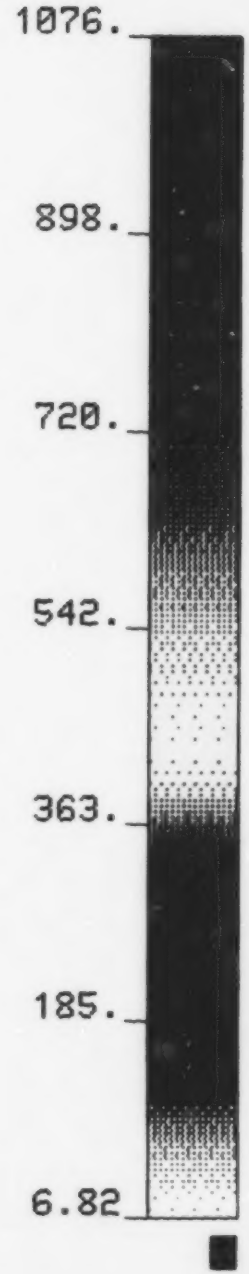

FIGURE 25

VON MISES IN THE OUTER LAYER STEEL REINFORCEMENT
AT 0.004 SECONDS (MPa)
(1/4 SCALE MODEL)

CIC 9M DROP
TIME= 0.004

89-298

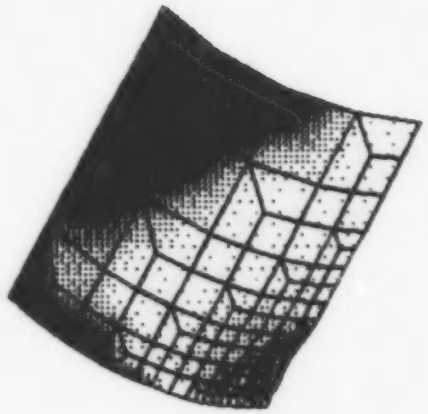

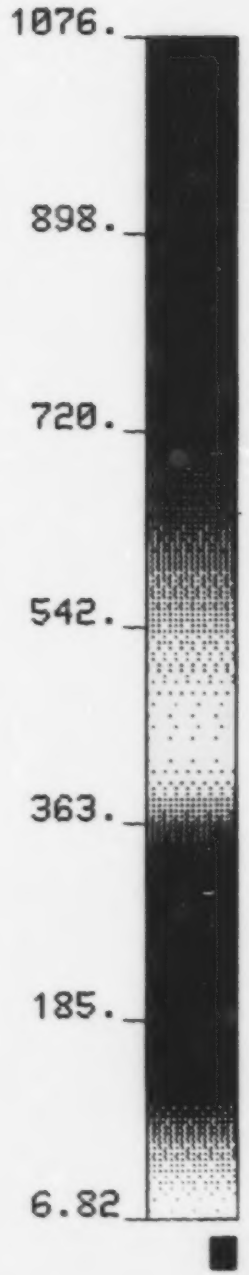

FIGURE 26

VON MISES STRESS IN THE INNER LAYER STEEL REINFORCEMENT
AT 0.004 SECONDS (MPa)
(1/4 SCALE MODEL)

CIC 9M DROP
TIME= 0.004

89-298

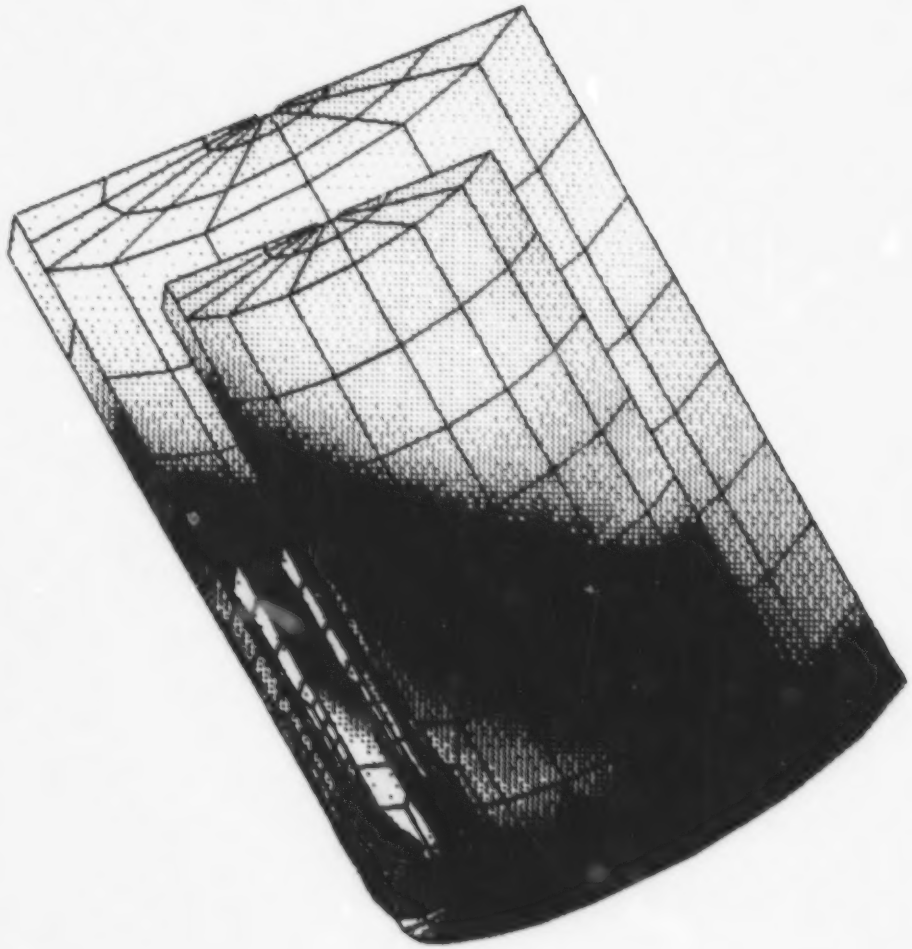

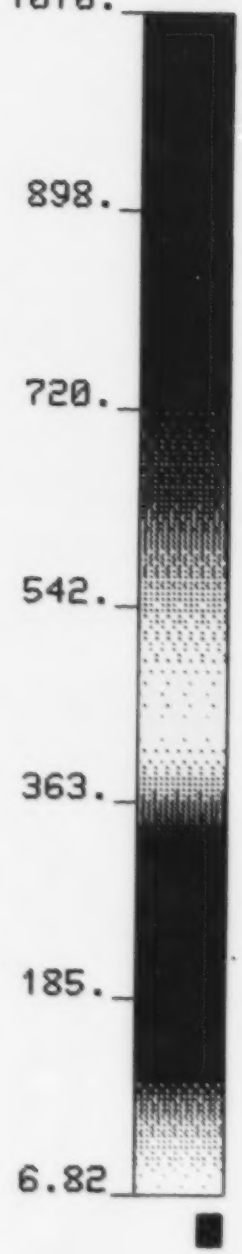

89-298

FIGURE 27

VON MISES STRESS IN THE LINERS AND REINFORCEMENTS AT
0.004 SECONDS (MPa)
(1/4 SCALE MODEL)

CIC 9M DROP
TIME= 0.004

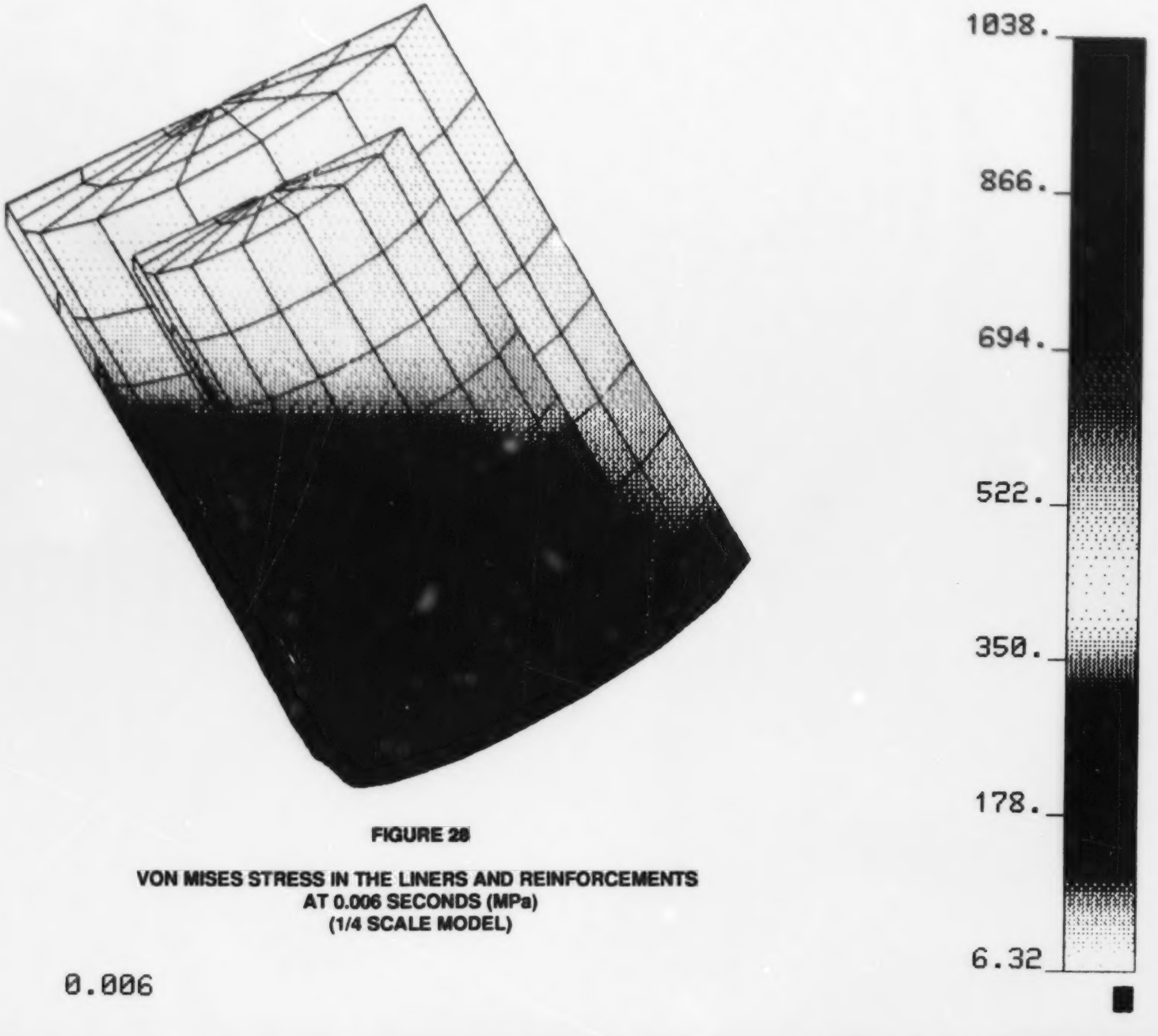

FIGURE 28

VON MISES STRESS IN THE LINERS AND REINFORCEMENTS AT 0.006 SECONDS (MPa) (1/4 SCALE MODEL)

41

89-298

FIGURE 29

VON MISES STRESS IN THE STEEL LID PLATE AT 0.004 SECONDS (MPa) (1/4 SCALE MODEL)

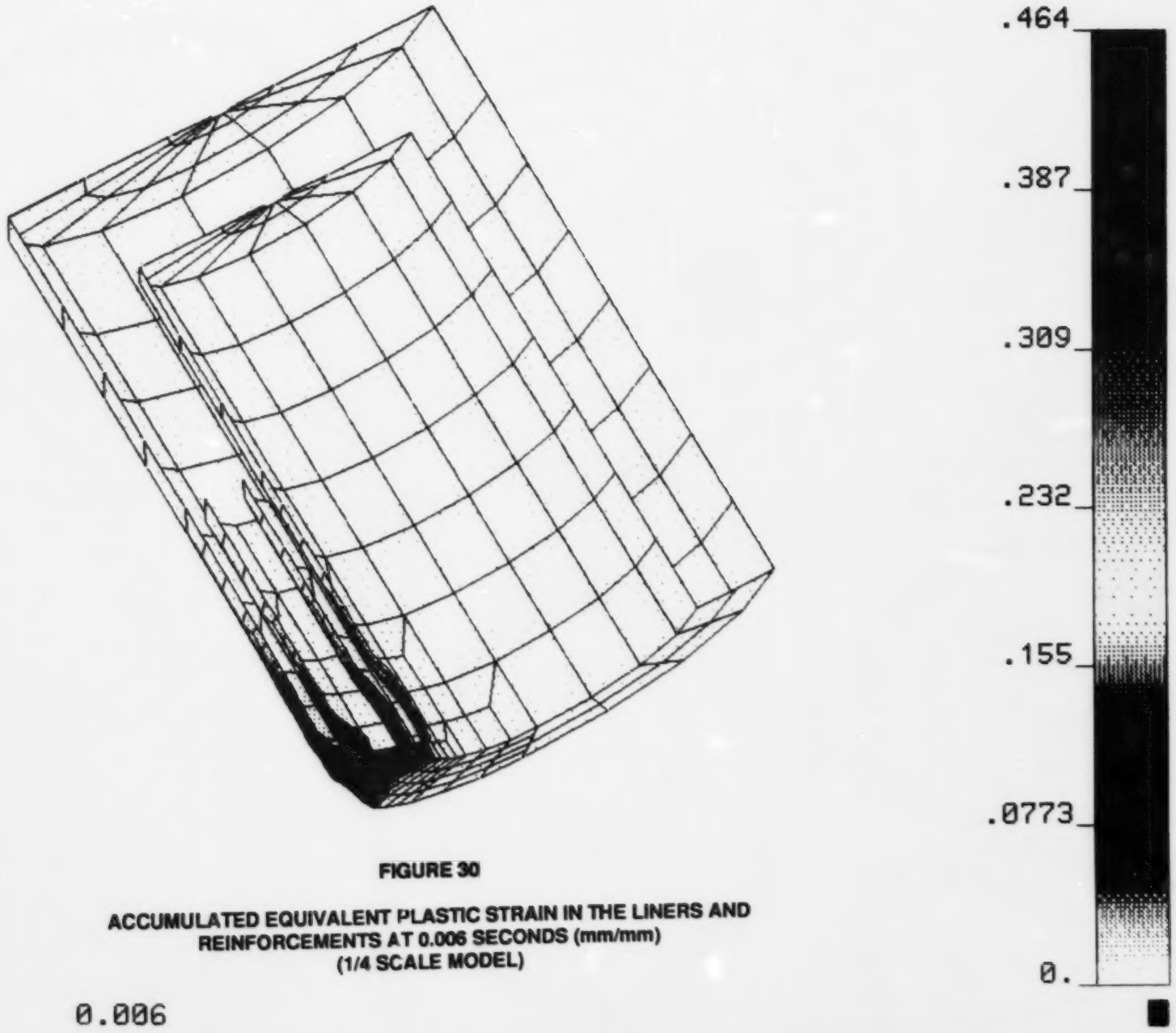

FIGURE 30

ACCUMULATED EQUIVALENT PLASTIC STRAIN IN THE LINERS AND REINFORCEMENTS AT 0.006 SECONDS (mm/mm) (1/4 SCALE MODEL)

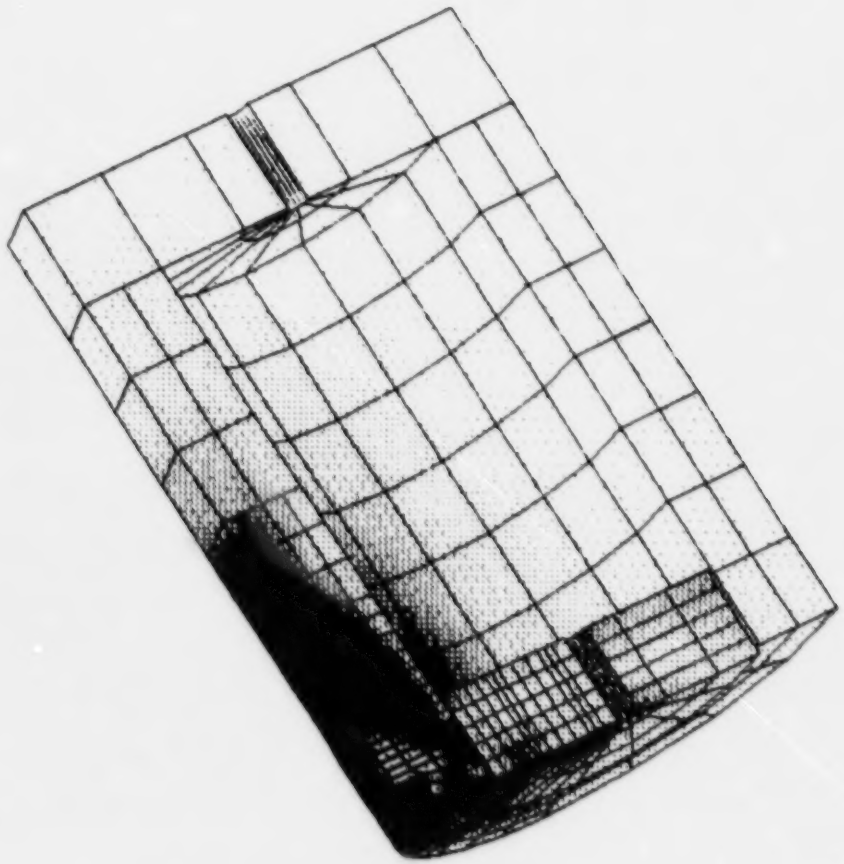

FIGURE 31

EFFECTIVE STRESS IN CONCRETE AT 0.002 SECONDS (MPa)
(1/4 SCALE MODEL)

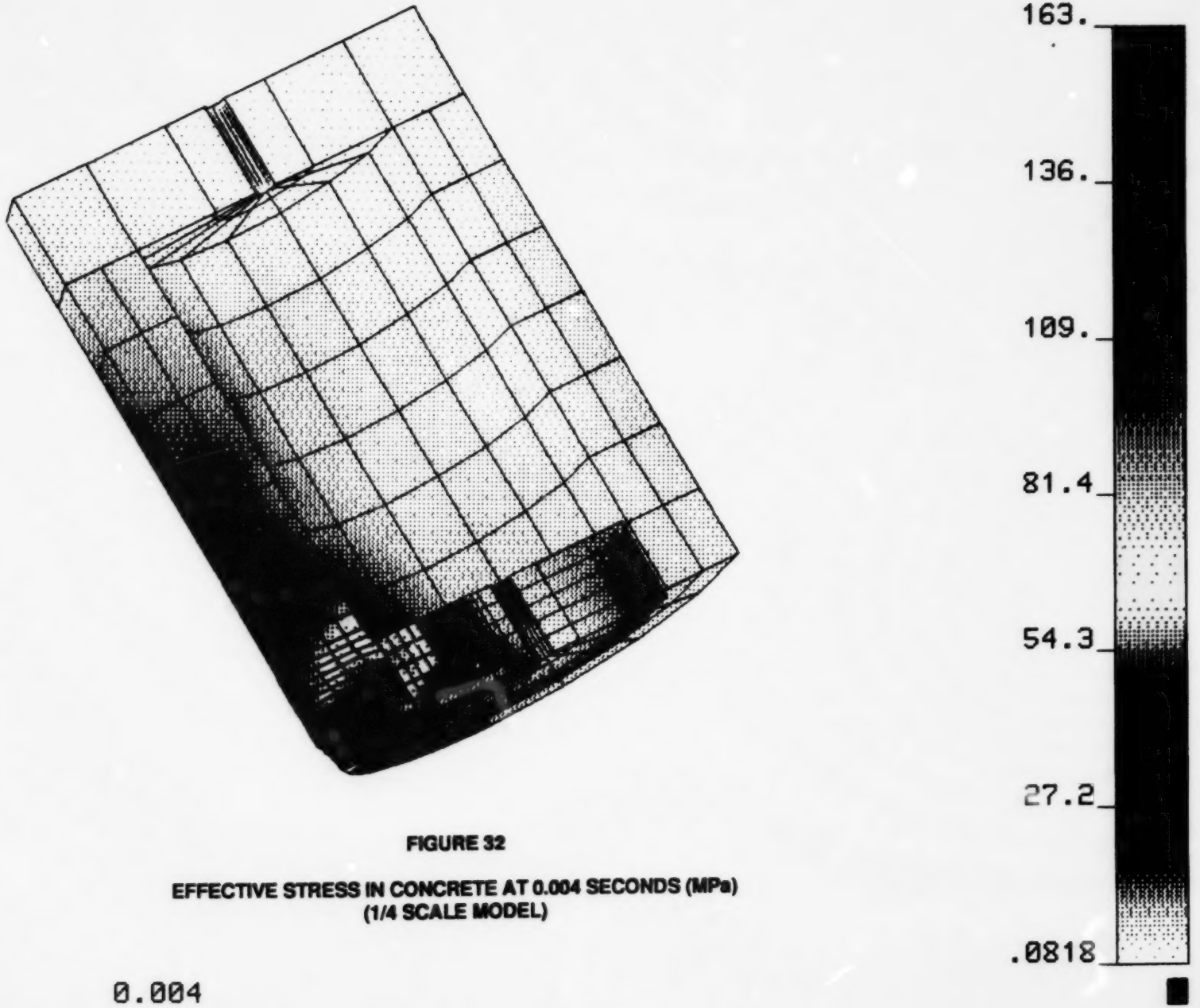

44

89-298

FIGURE 32

EFFECTIVE STRESS IN CONCRETE AT 0.004 SECONDS (MPa)
(1/4 SCALE MODEL)

FIGURE 33

EFFECTIVE STRESS IN CONCRETE AT 0.006 SECONDS (MPa)
(1/4 SCALE MODEL)

89-298

CIC 9M DROP
TTME= 0.006

FIGURE 34

ACCUMULATED EQUIVALENT PLASTIC STRAIN IN CONCRETE AT 0.006 SECONDS (mm/mm) (1/4 SCALE MODEL)

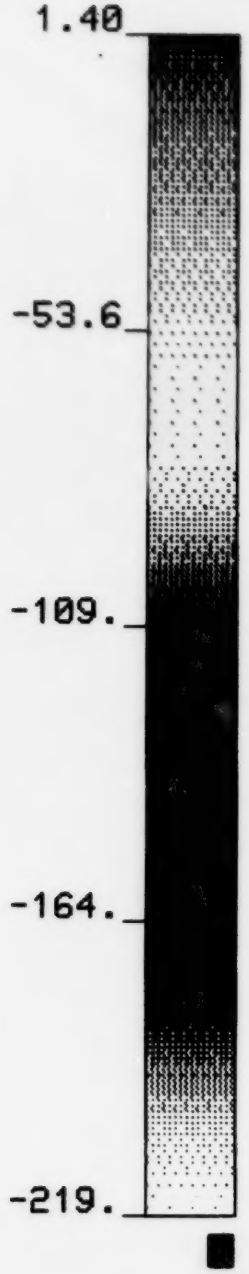

89-298

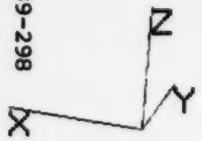

FIGURE 35

HYDROSTATIC PRESSURE IN CONCRETE AT 0.004 SECONDS (MPa)
(1/4 SCALE MODEL)

CIC 9M DROP
TIME= 0.004

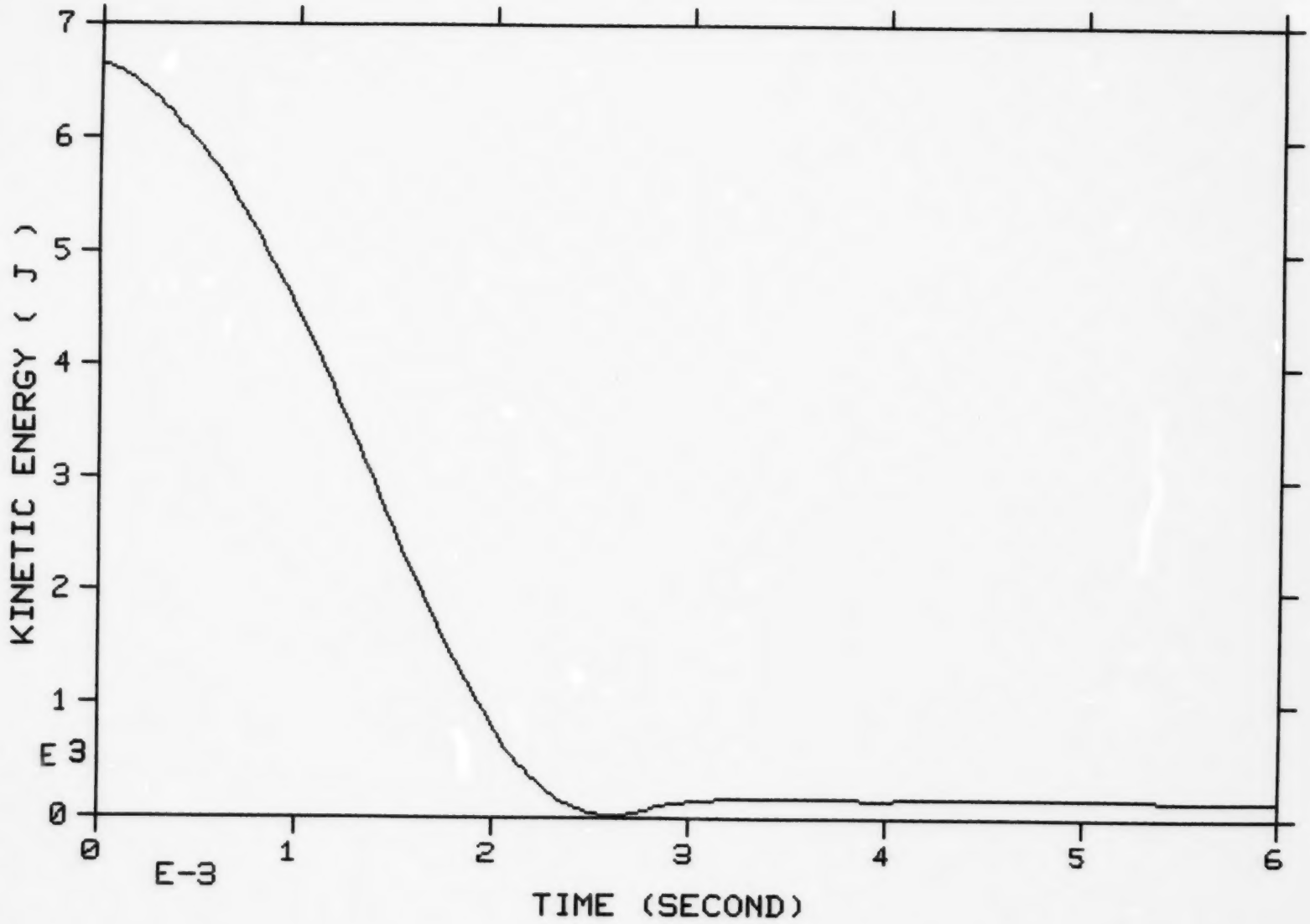

FIGURE 36

KINETIC ENERGY TIME HISTORY OF THE CIC
(1/8 SCALE MODEL)

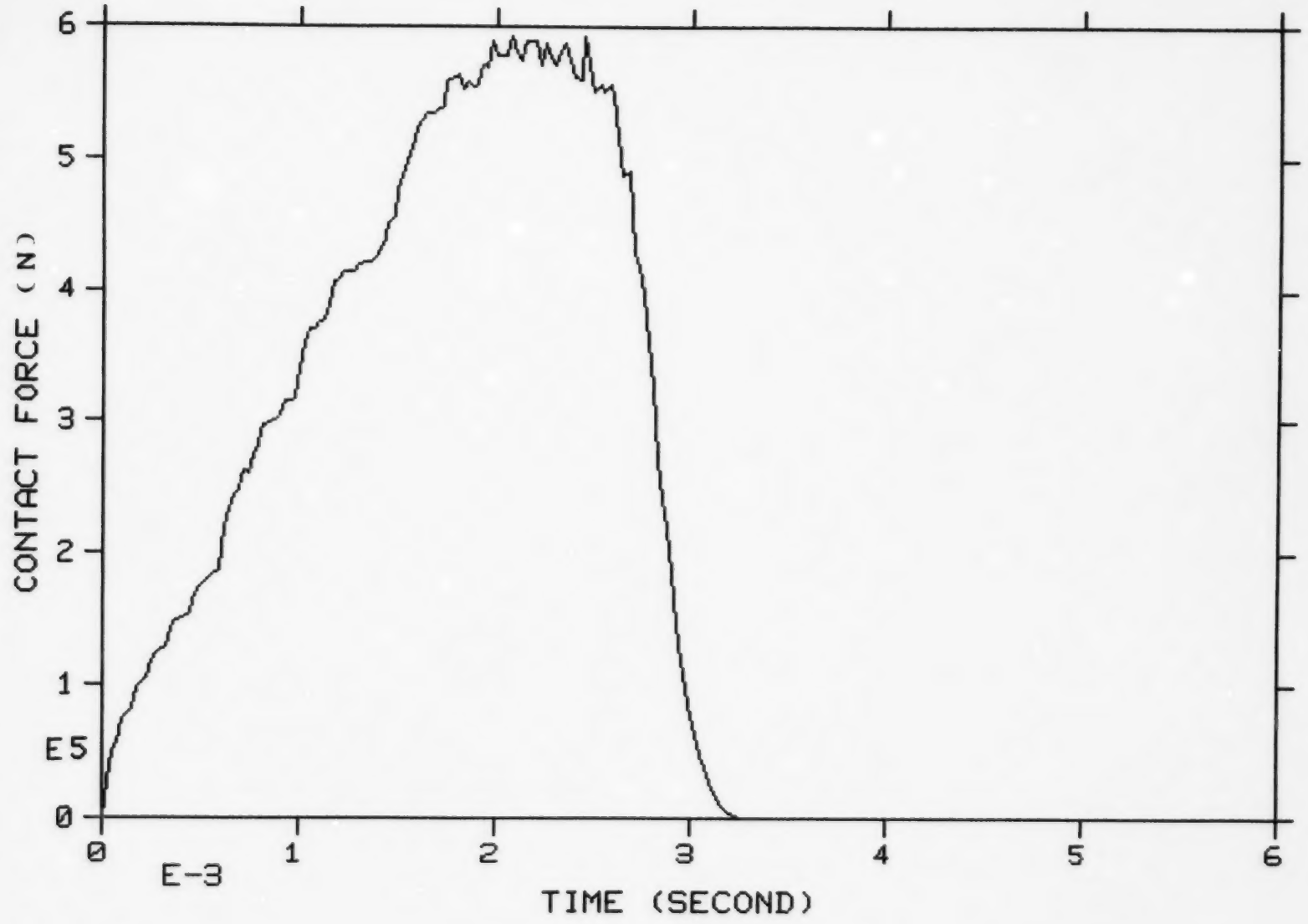

FIGURE 37

CONTACT FORCE TIME HISTORY OF THE CIC (1/8 SCALE MODEL)

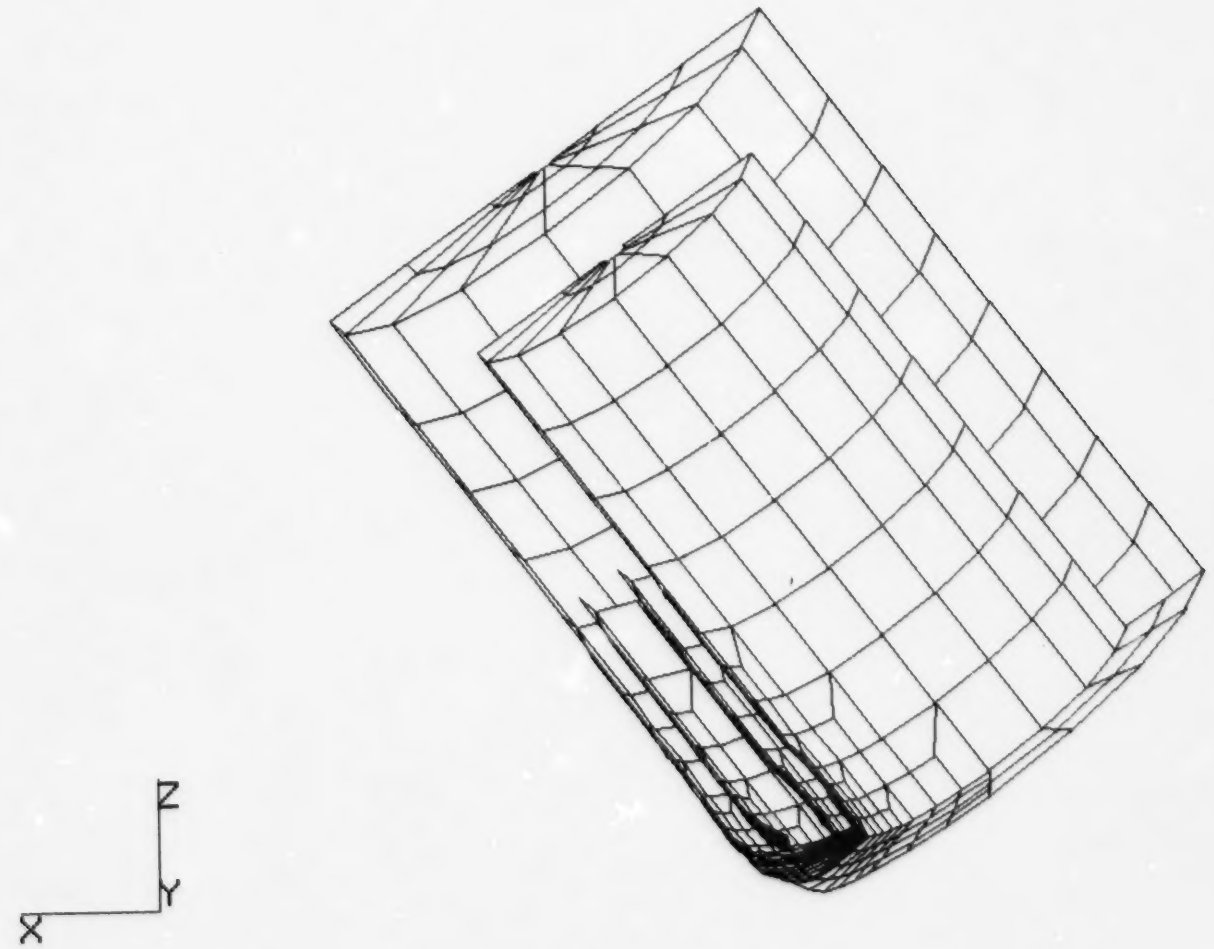

FIGURE 38

DEFORMATION OF THE STEEL LINERS AND REINFORCEMENTS AT 0.004 SECONDS
(1/8 SCALE MODEL)

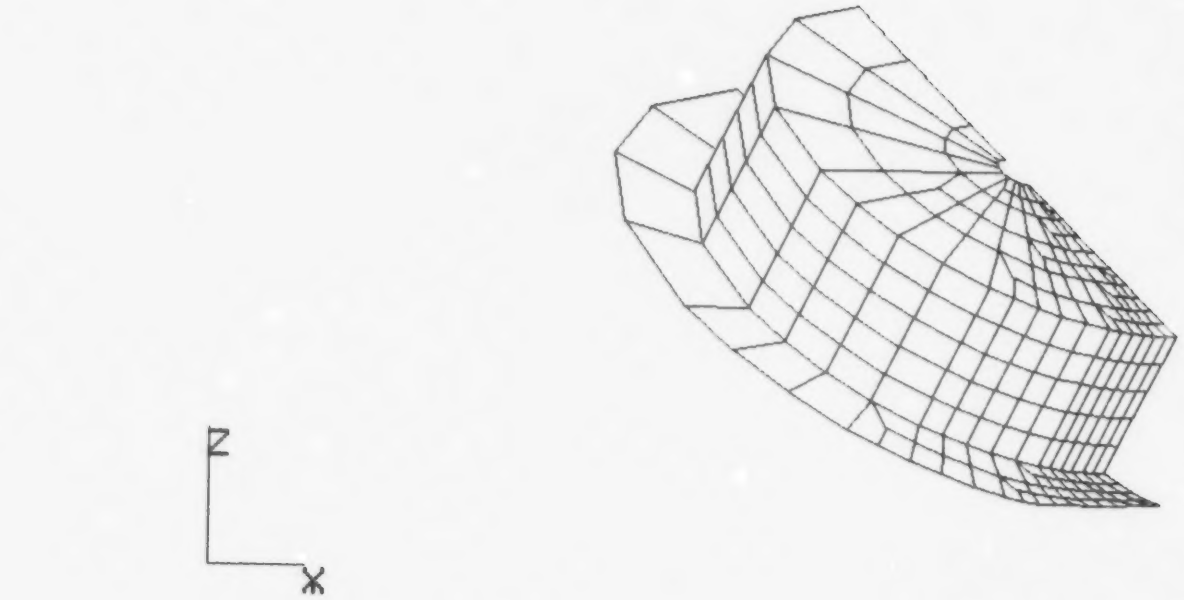

FIGURE 39

DEFORMATION OF THE STEEL LID PLATE AT 0.004 SECONDS (1/8 SCALE MODEL)

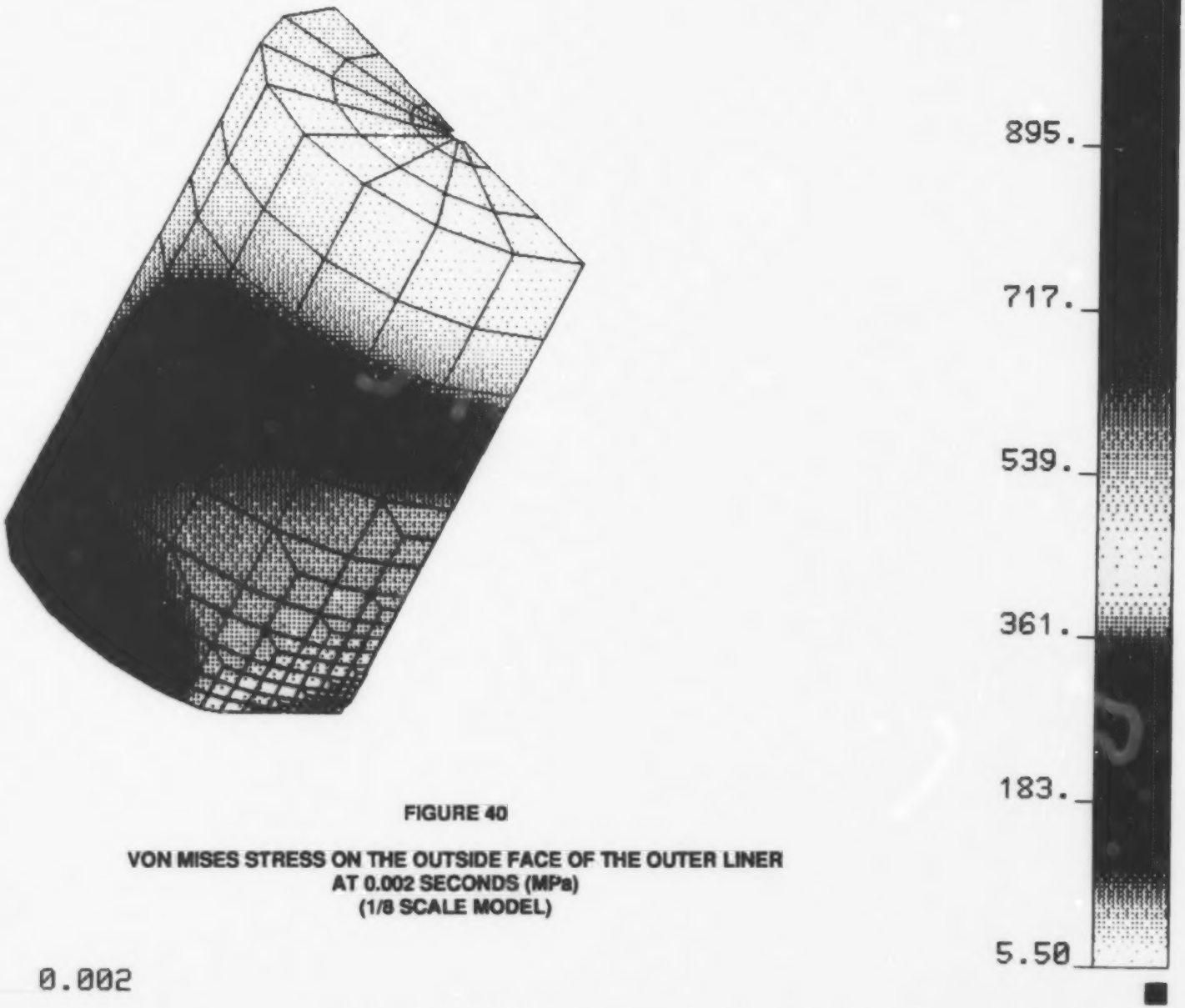

FIGURE 40

VON MISES STRESS ON THE OUTSIDE FACE OF THE OUTER LINER
AT 0.002 SECONDS (MPa)
(1/8 SCALE MODEL)

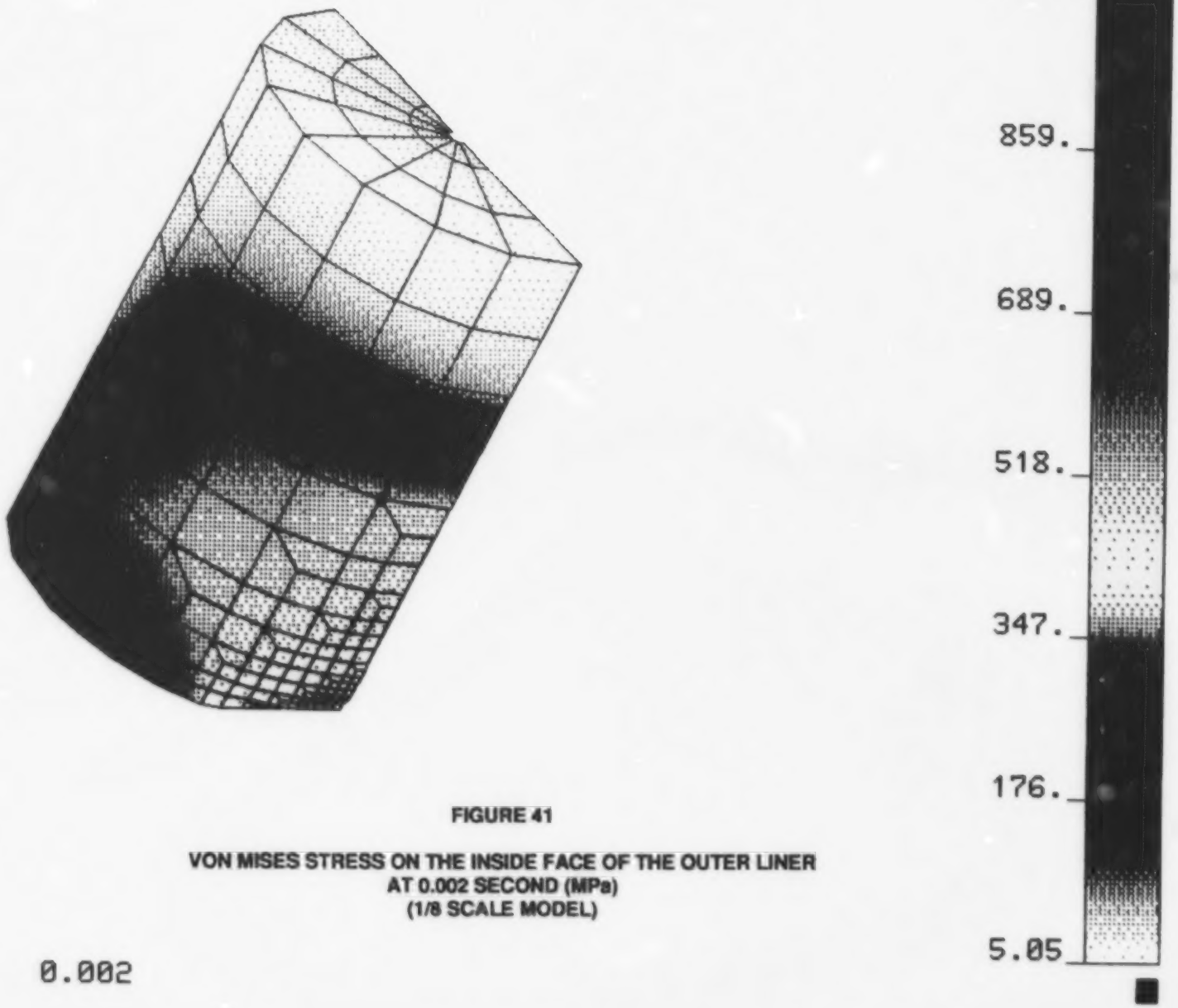

FIGURE 41

VON MISES STRESS ON THE INSIDE FACE OF THE OUTER LINER AT 0.002 SECOND (MPa) (1/8 SCALE MODEL)

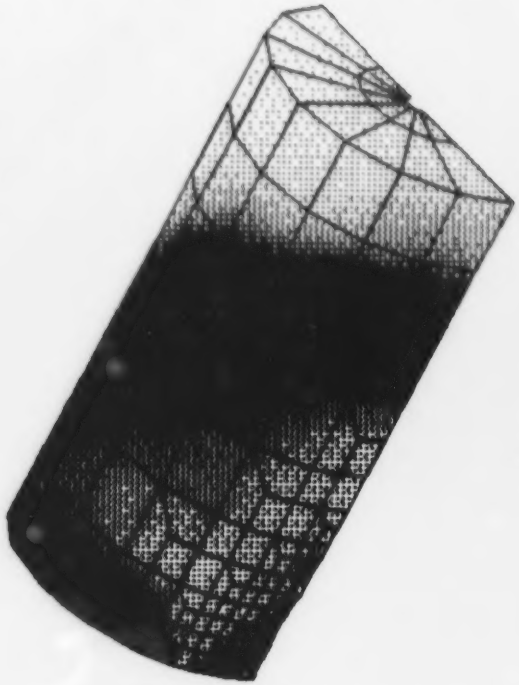

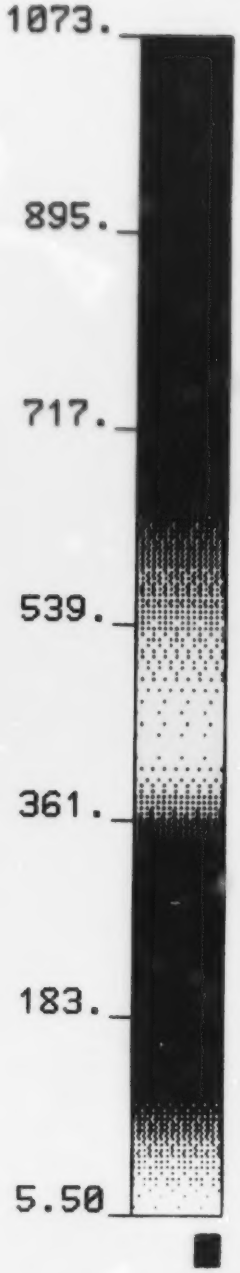

CIC 9M DROP
TIME= 0.002

54

89-298

FIGURE 42

VON MISES STRESS IN THE INNER LINER AT 0.002 SECONDS (MPa)
(1/8 SCALE MODEL)

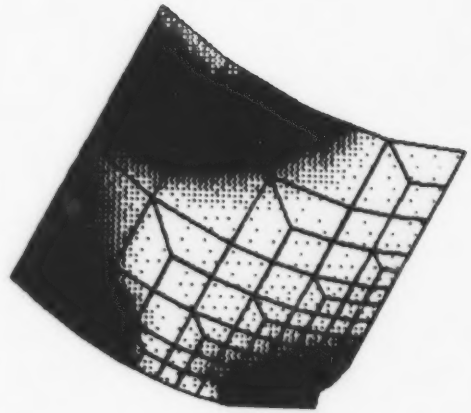

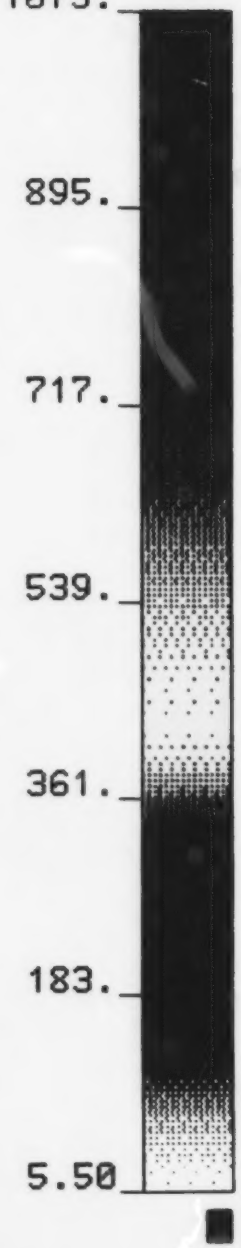

55

89-298

FIGURE 43

VON MISES STRESS IN THE OUTER LAYER STEEL REINFORCEMENT AT 0.002 SECONDS (MPa) (1/8 SCALE MODEL)

CIC 9M DROP
TIME= 0.002

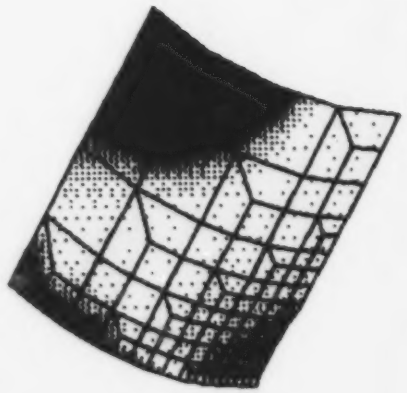

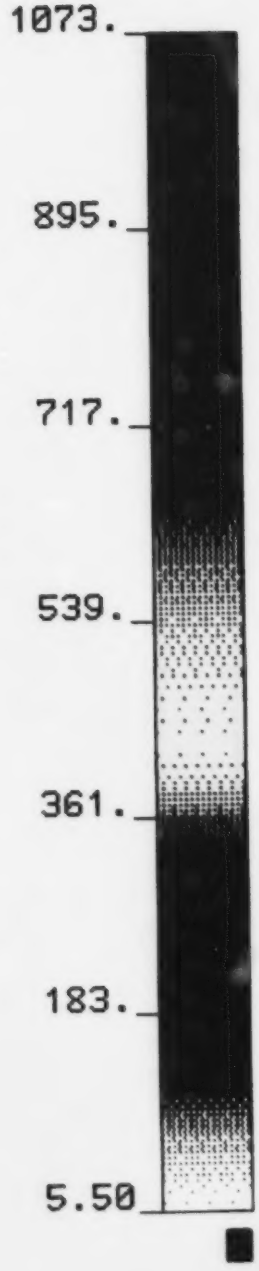

89-298

56

FIGURE 44

VON MISES STRESS IN THE INNER LAYER STEEL REINFORCEMENT
AT 0.002 SECONDS (MPa)
(1/8 SCALE MODEL)

CIC 9M DROP
TIME= 0.002

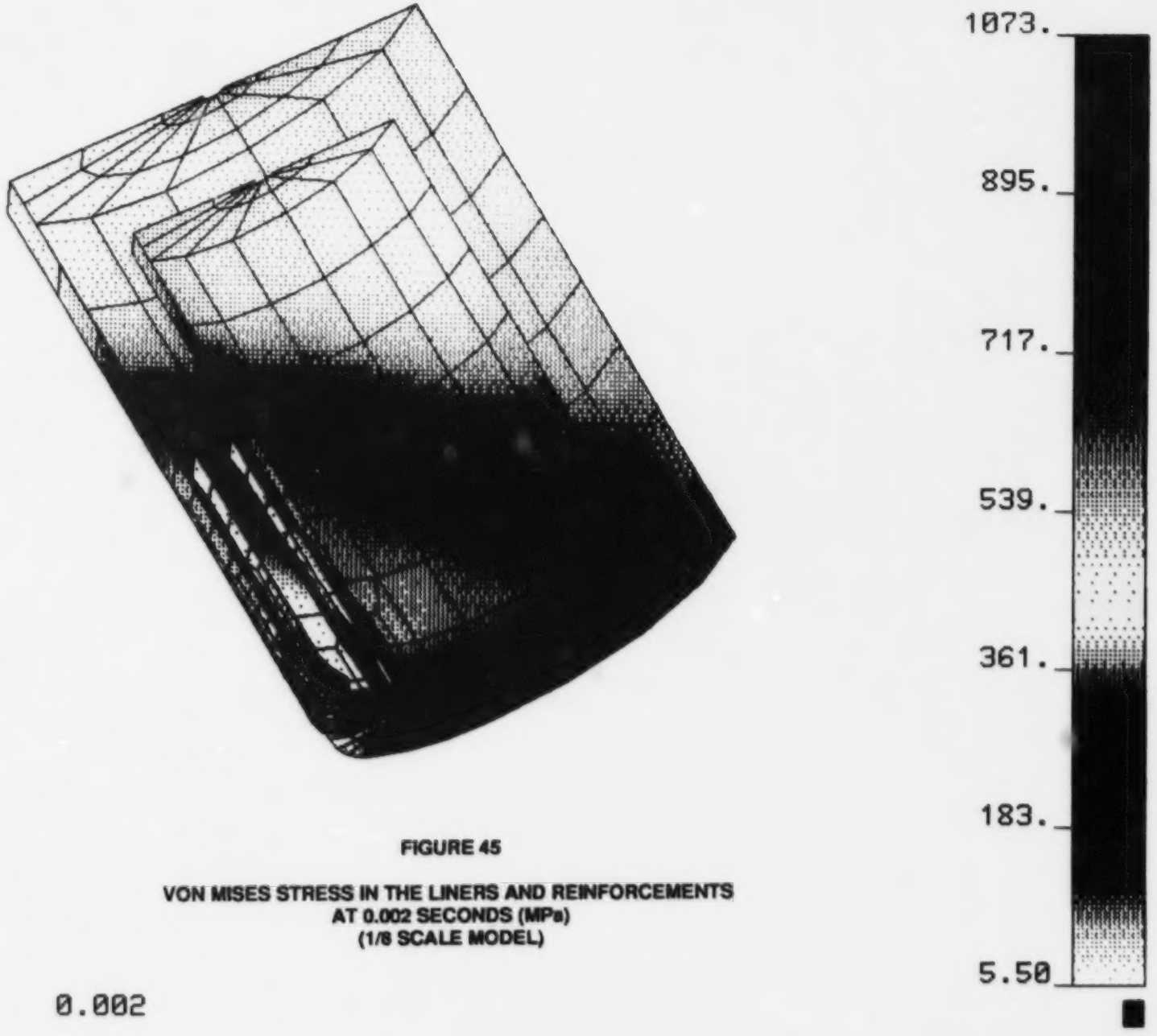

FIGURE 45

VON MISES STRESS IN THE LINERS AND REINFORCEMENTS AT 0.002 SECONDS (MPa) (1/8 SCALE MODEL)

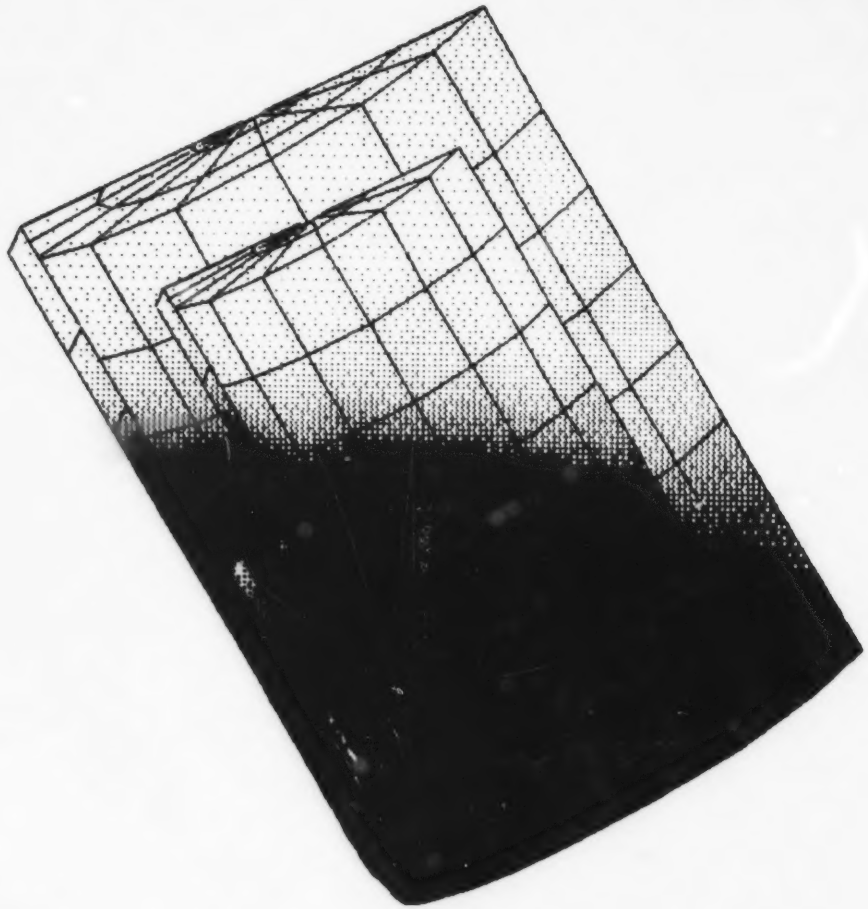

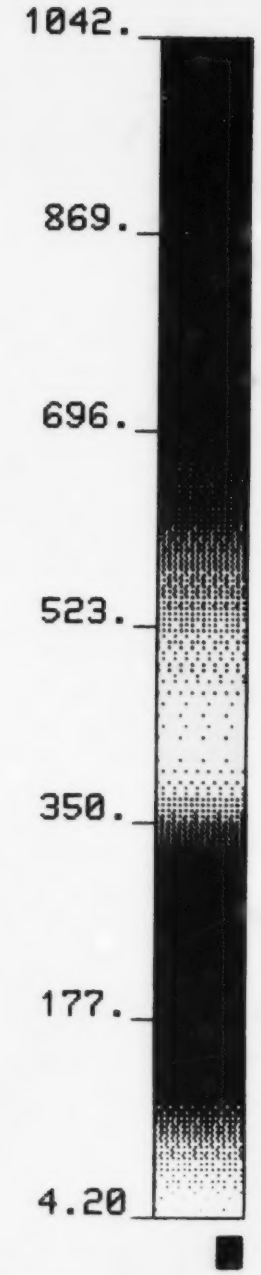

89-298

CIC 9M DROP
TIME= 0.003

FIGURE 46

VON MISES STRESS IN THE LINERS AND REINFORCEMENTS AT 0.003 SECONDS (MPa) (1/8 SCALE MODEL)

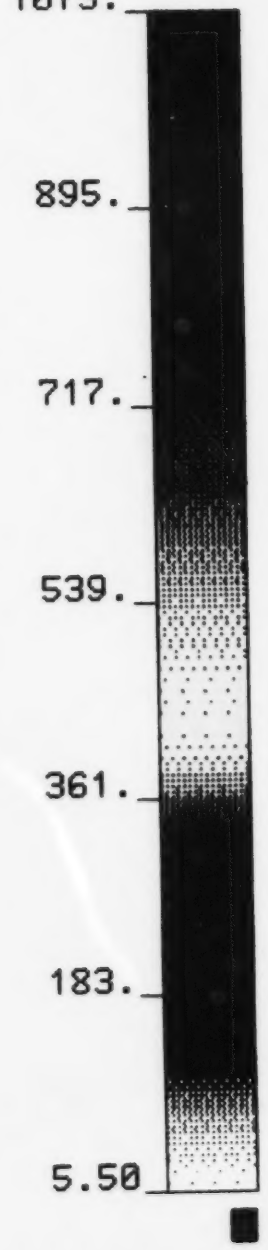

59

89-298

Z
X

CIC 9M DROP
TIME= 0.002

FIGURE 47

VON MISES STRESS IN THE STEEL LID PLATE AT 0.002 SECONDS (MPa) (1/8 SCALE MODEL)

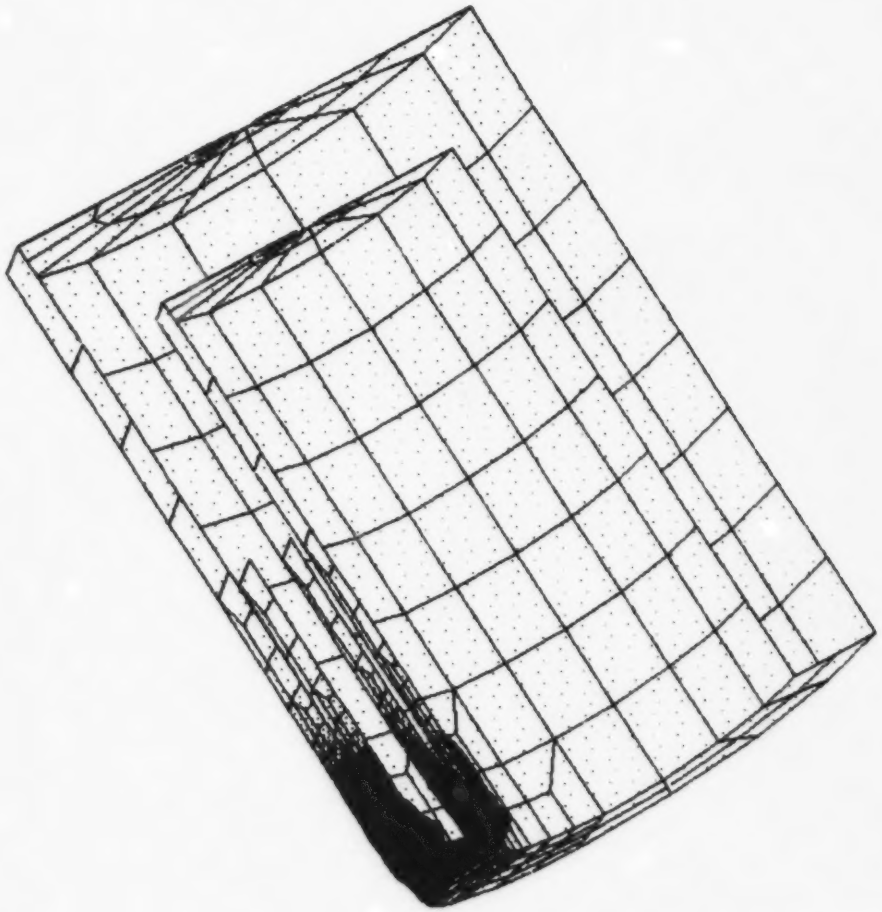

FIGURE 48

ACCUMULATED EQUIVALENT PLASTIC STRAIN IN THE LINERS AND REINFORCEMENTS AT 0.003 SECONDS (mm/mm) (1/8 SCALE MODEL)

FIGURE 49

EFFECTIVE STRESS IN CONCRETE AT 0.002 SECONDS (MPa)
(1/8 SCALE MODEL)

FIGURE 50

EFFECTIVE STRESS IN CONCRETE AT 0.003 SECONDS (MPa)
(1/8 SCALE MODEL)

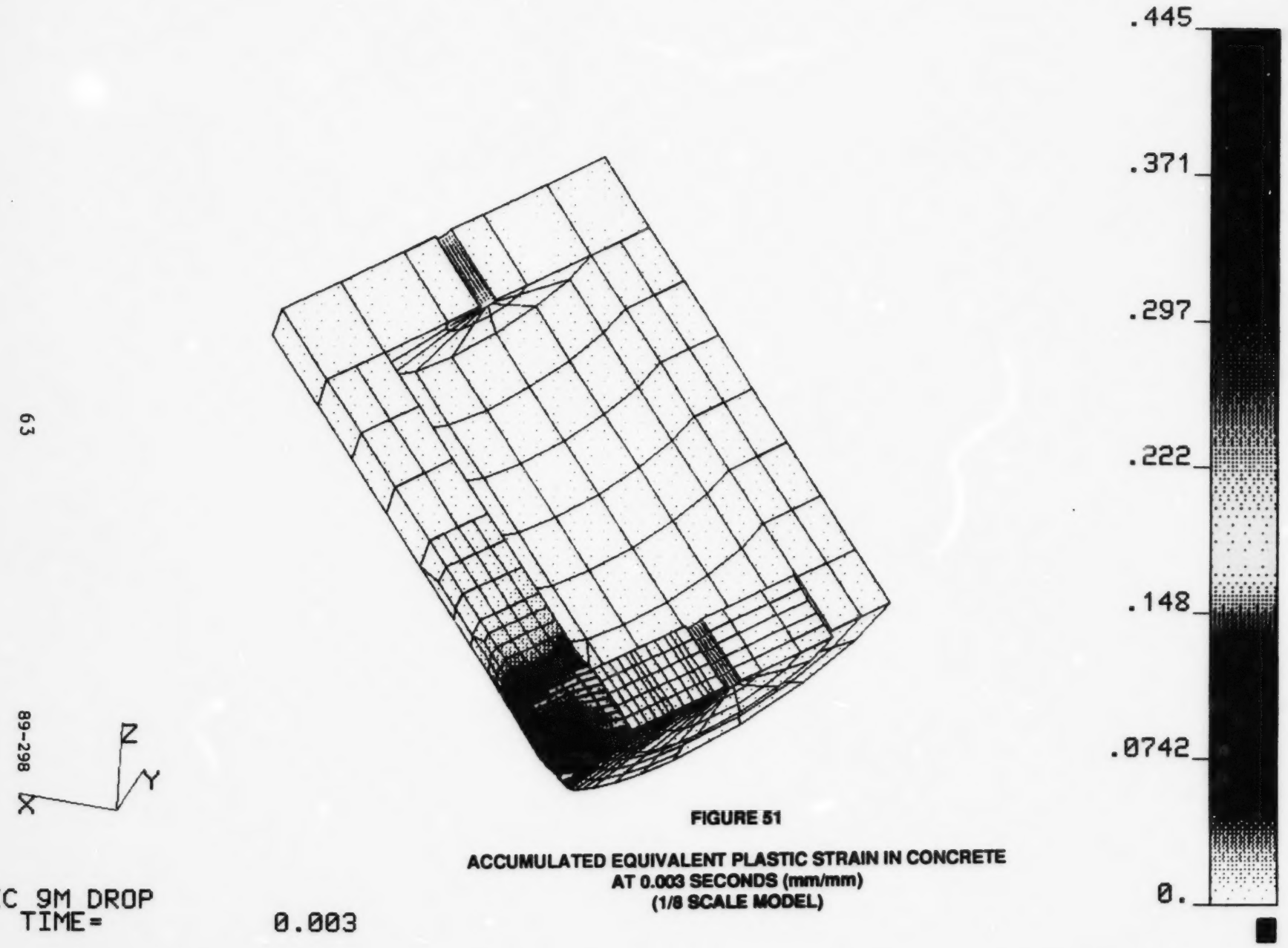

FIGURE 51

ACCUMULATED EQUIVALENT PLASTIC STRAIN IN CONCRETE AT 0.003 SECONDS (mm/mm) (1/8 SCALE MODEL)

FIGURE 52

HYDROSTATIC PRESSURE IN CONCRETE AT 0.002 SECONDS (MPa)
(1/8 SCALE MODEL)

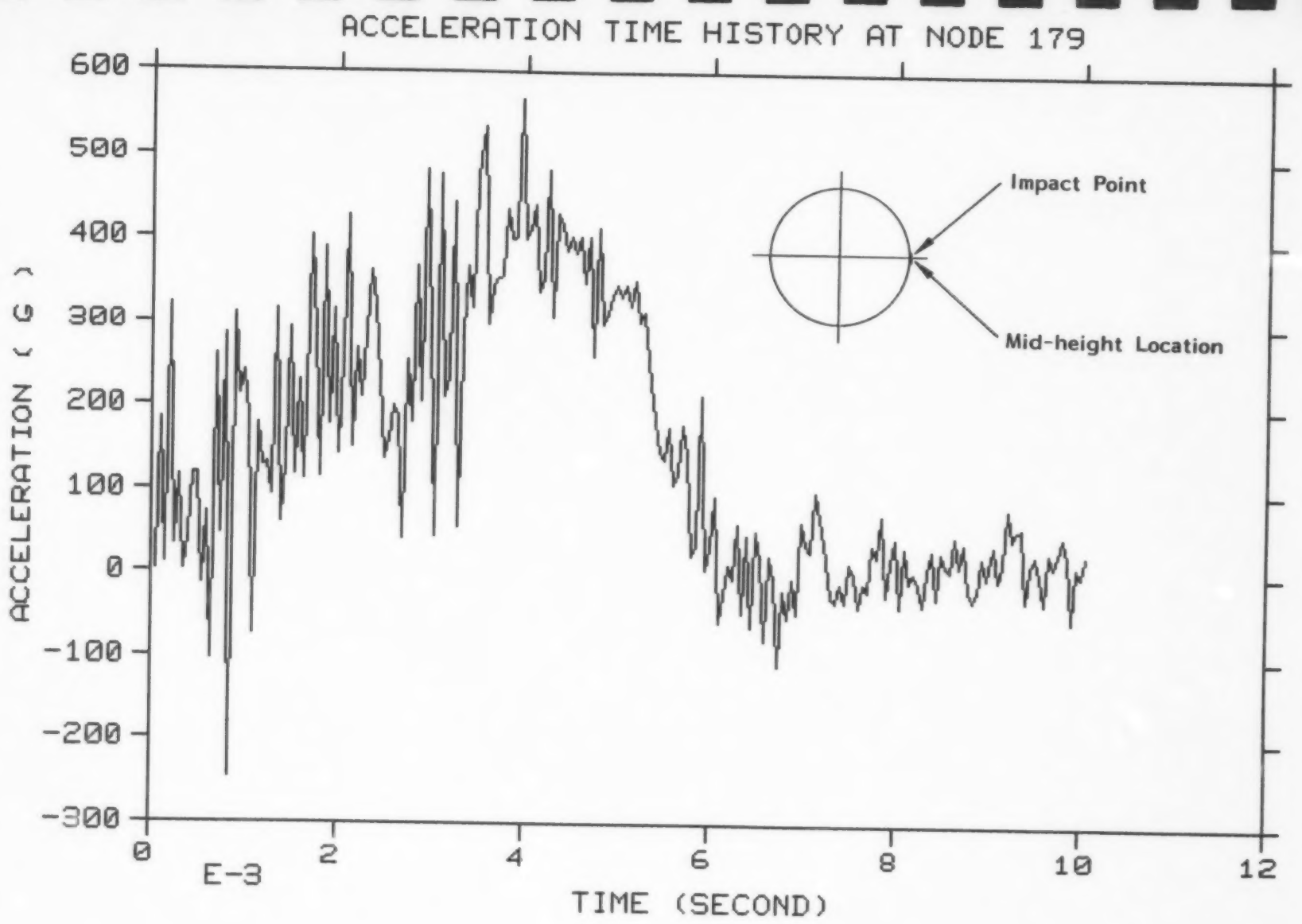

FIGURE 53

ACCELERATION TIME HISTORY AT MID-HEIGHT OF OUTER LINER
DIRECTLY ABOVE IMPACT POINT
(1/4 SCALE MODEL)

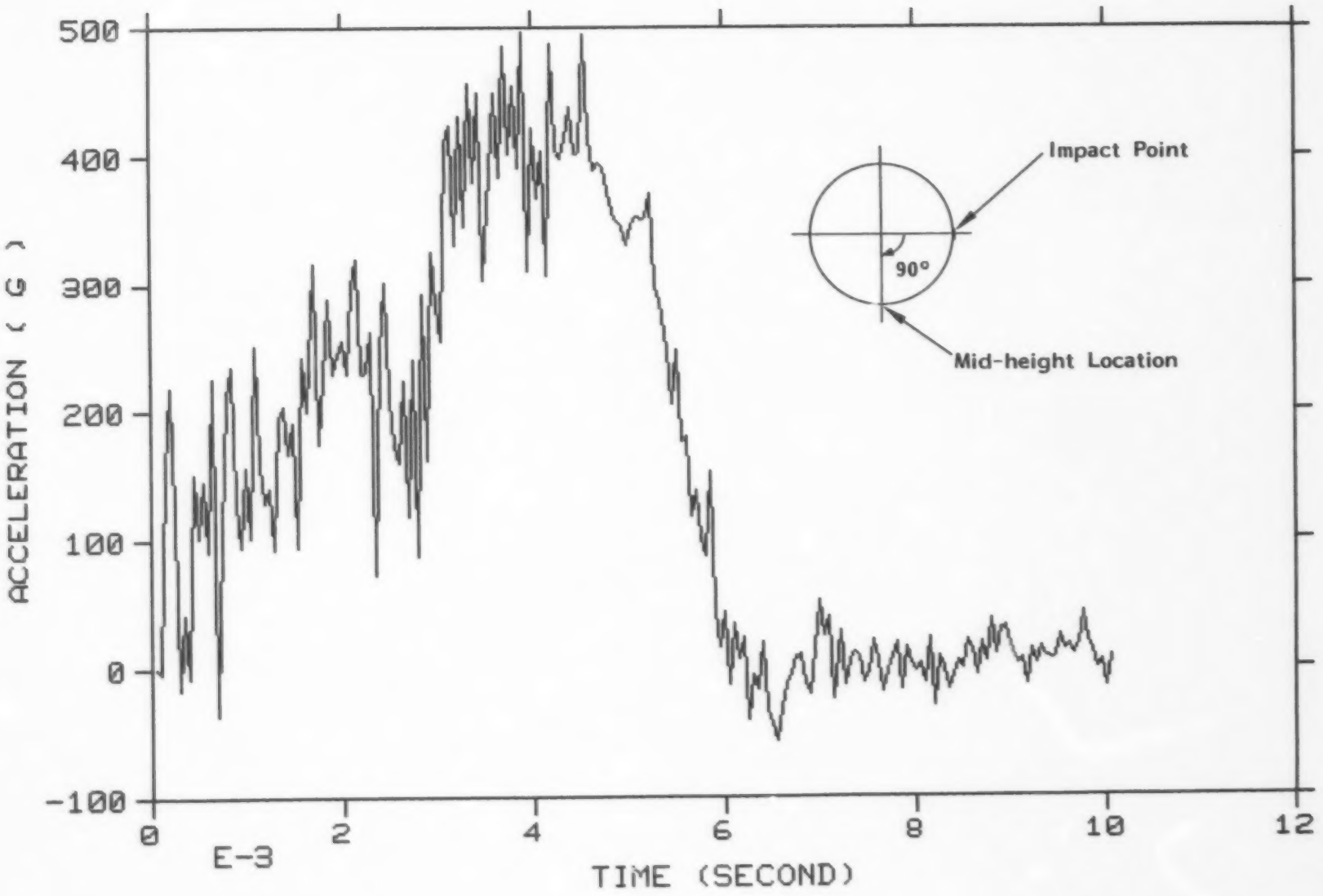

FIGURE 54

ACCELERATION TIME HISTORY AT MID-HEIGHT OF OUTER LINER
AT 90° FROM IMPACT POINT
(1/4 SCALE MODEL)

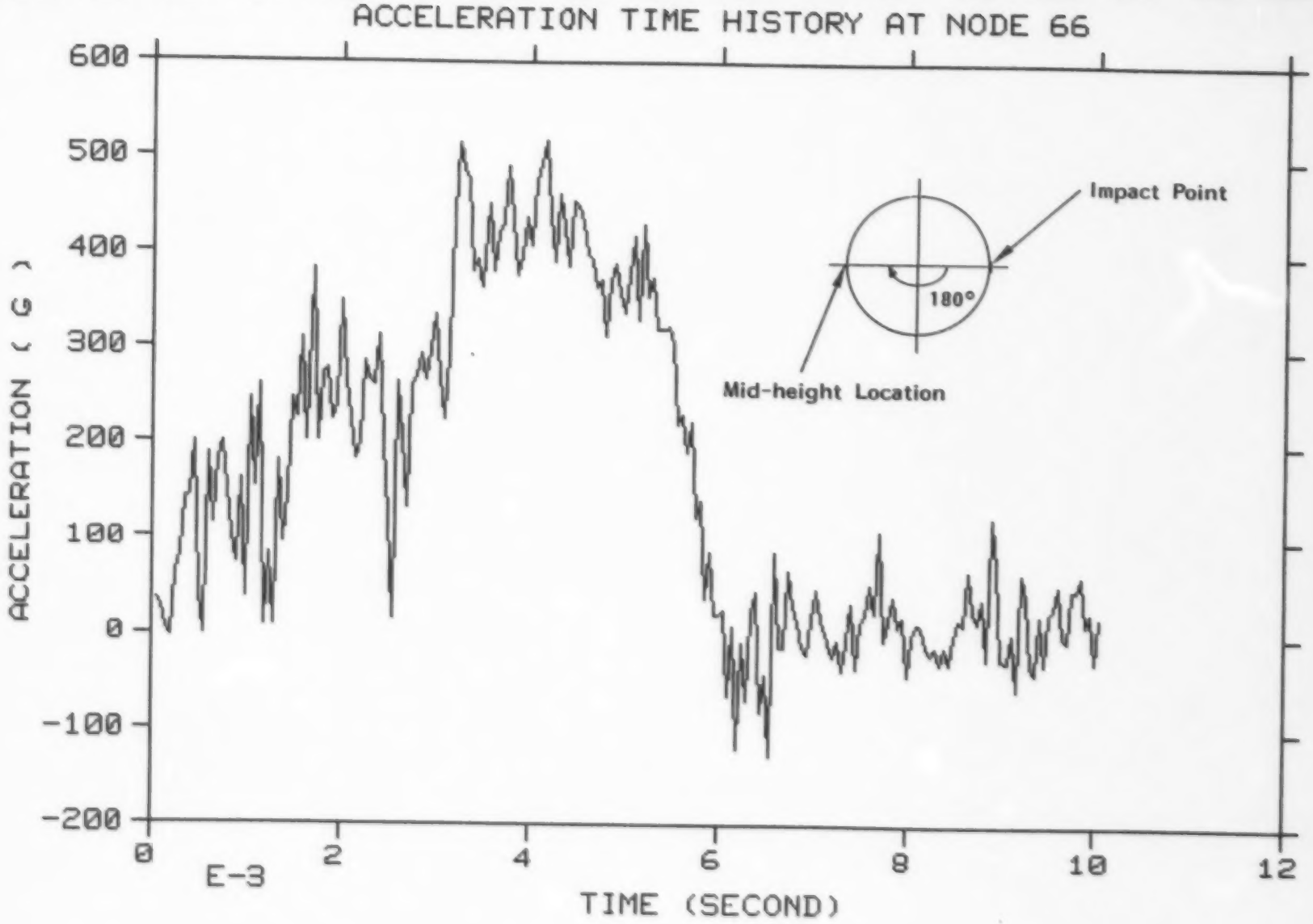

FIGURE 55

ACCELERATION TIME HISTORY AT MID-HEIGHT OF OUTER LINER AT 180° FROM IMPACT POINT (1/4 SCALE MODEL)

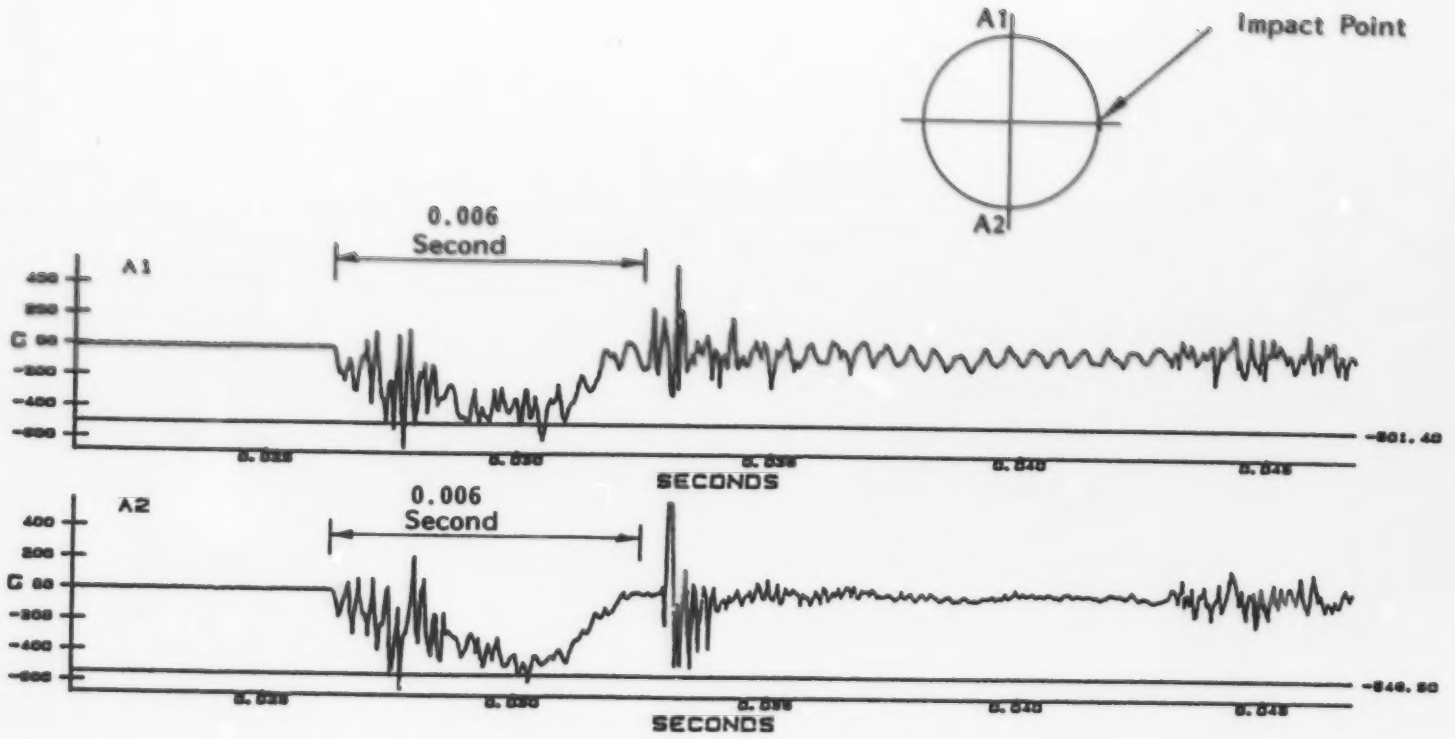

FIGURE 56
ACCELEROMETER DATA AT MID-HEIGHT OF OUTER LINER (UNITS = G's)
(1/4 SCALE MODEL)

89-298
182172-RD

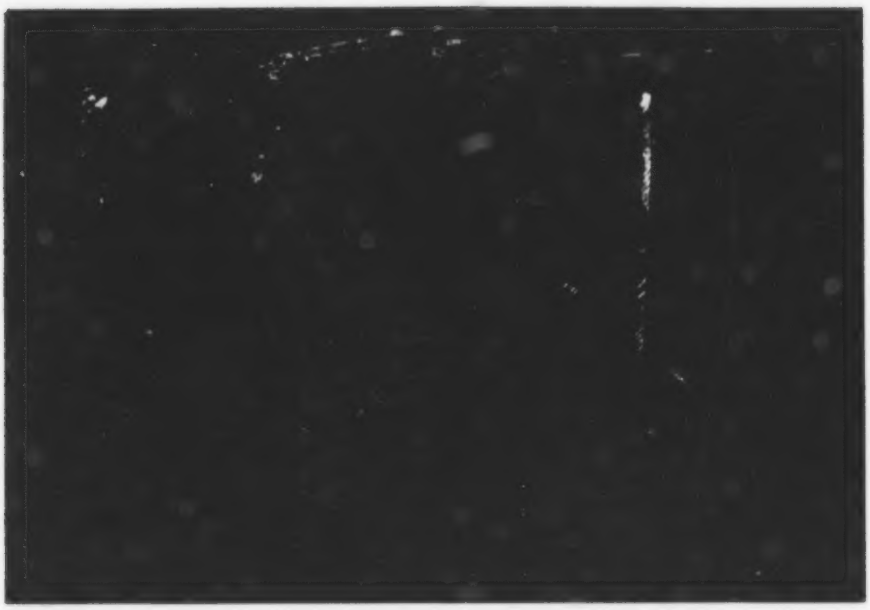

FIGURE 57(a)

TOP CORNER DAMAGE OF 1/4 SCALE MODEL

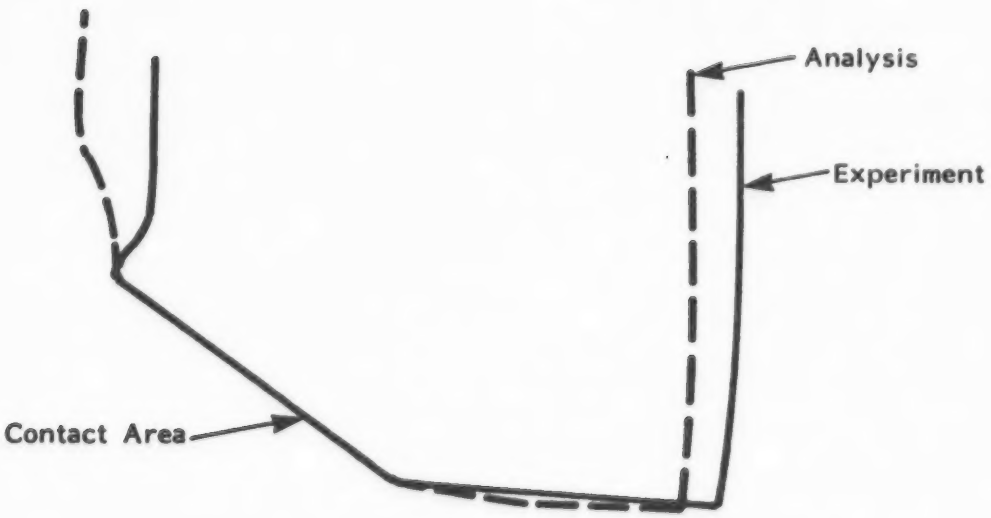

FIGURE 57(b)

COMPARISON OF TOP CORNER DEFORMATION
(1/4 SCALE MODEL)

182166-RD

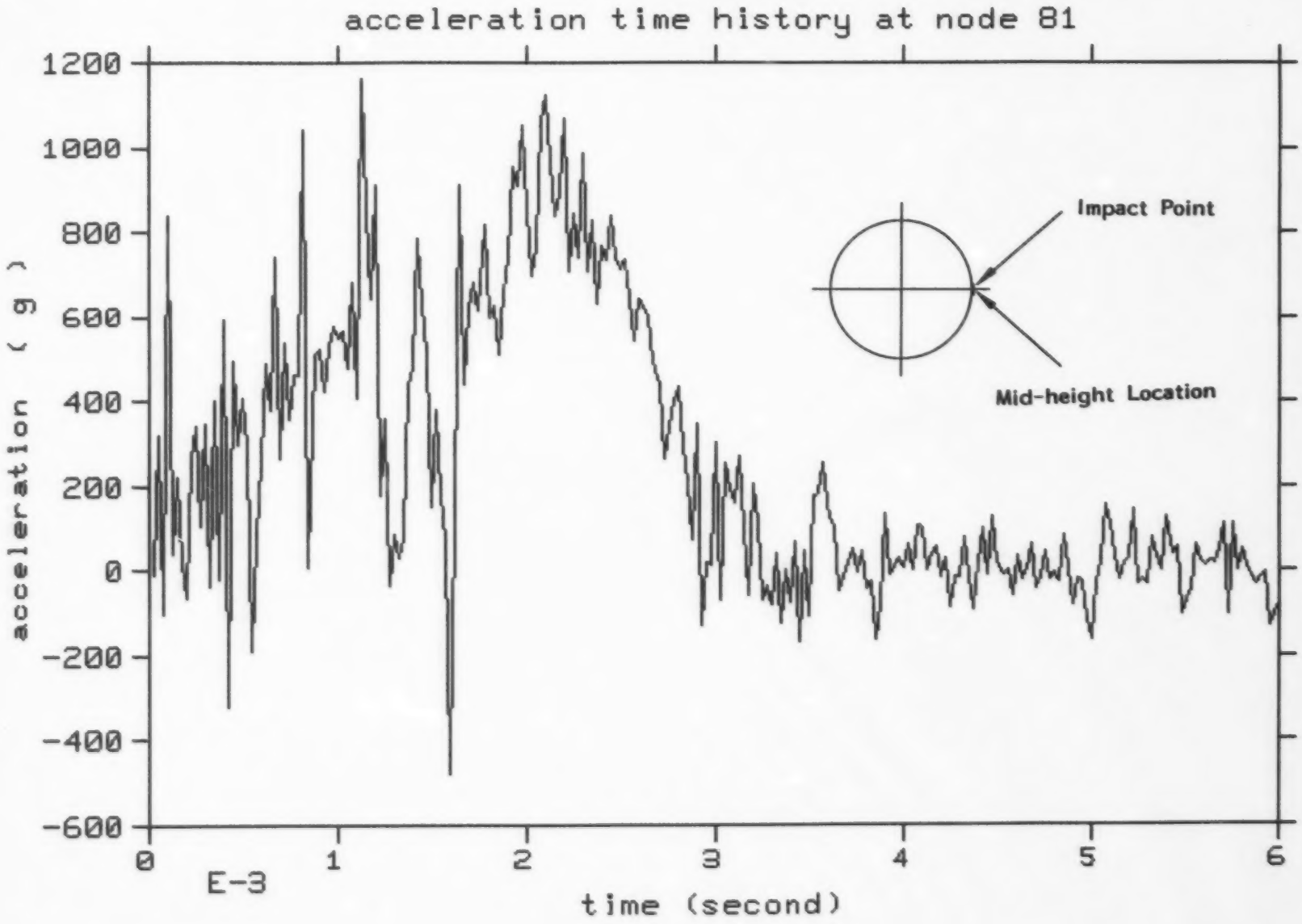

FIGURE 58

ACCELERATION TIME HISTORY AT MID-HEIGHT OF OUTER LINER
DIRECTLY ABOVE IMPACT POINT
(1/8 SCALE MODEL)

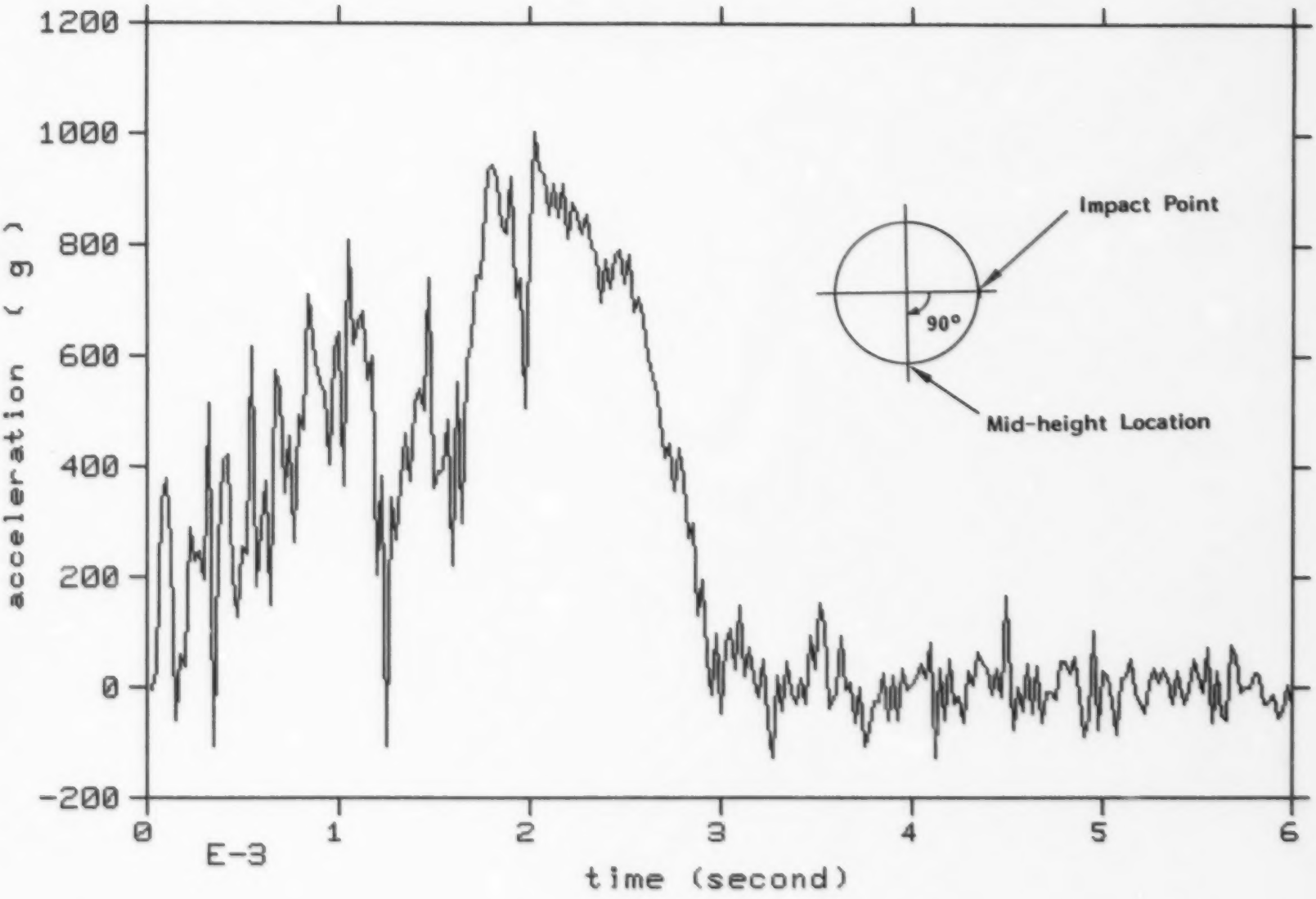

FIGURE 59

ACCELERATION TIME HISTORY AT MID-HEIGHT OF OUTER LINER
AT 90° FROM IMPACT POINT
(1/8 SCALE MODEL)

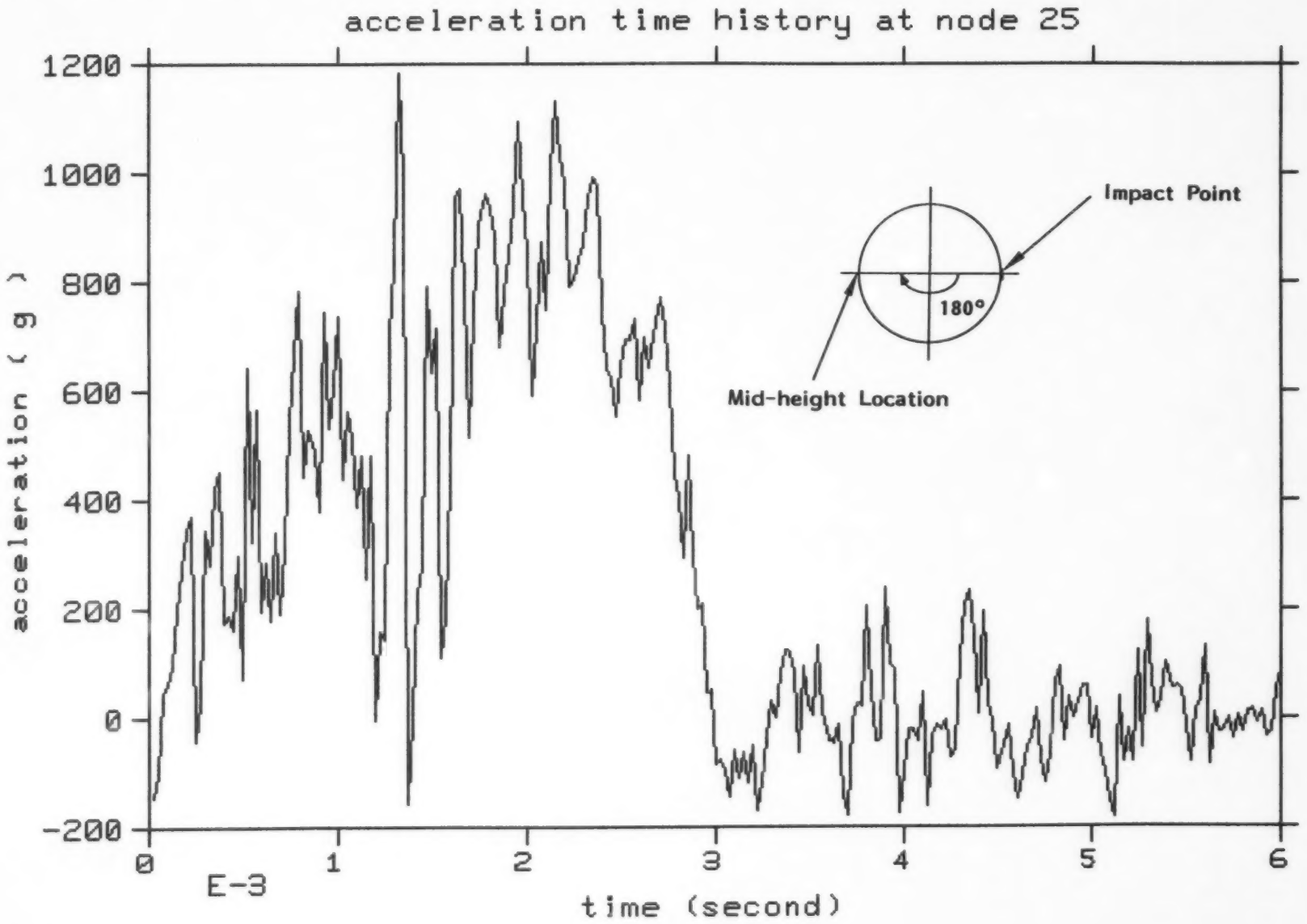

FIGURE 60

ACCELERATION TIME HISTORY AT MID-HEIGHT OF OUTER LINER
AT 180° FROM IMPACT POINT
(1/8 SCALE MODEL)

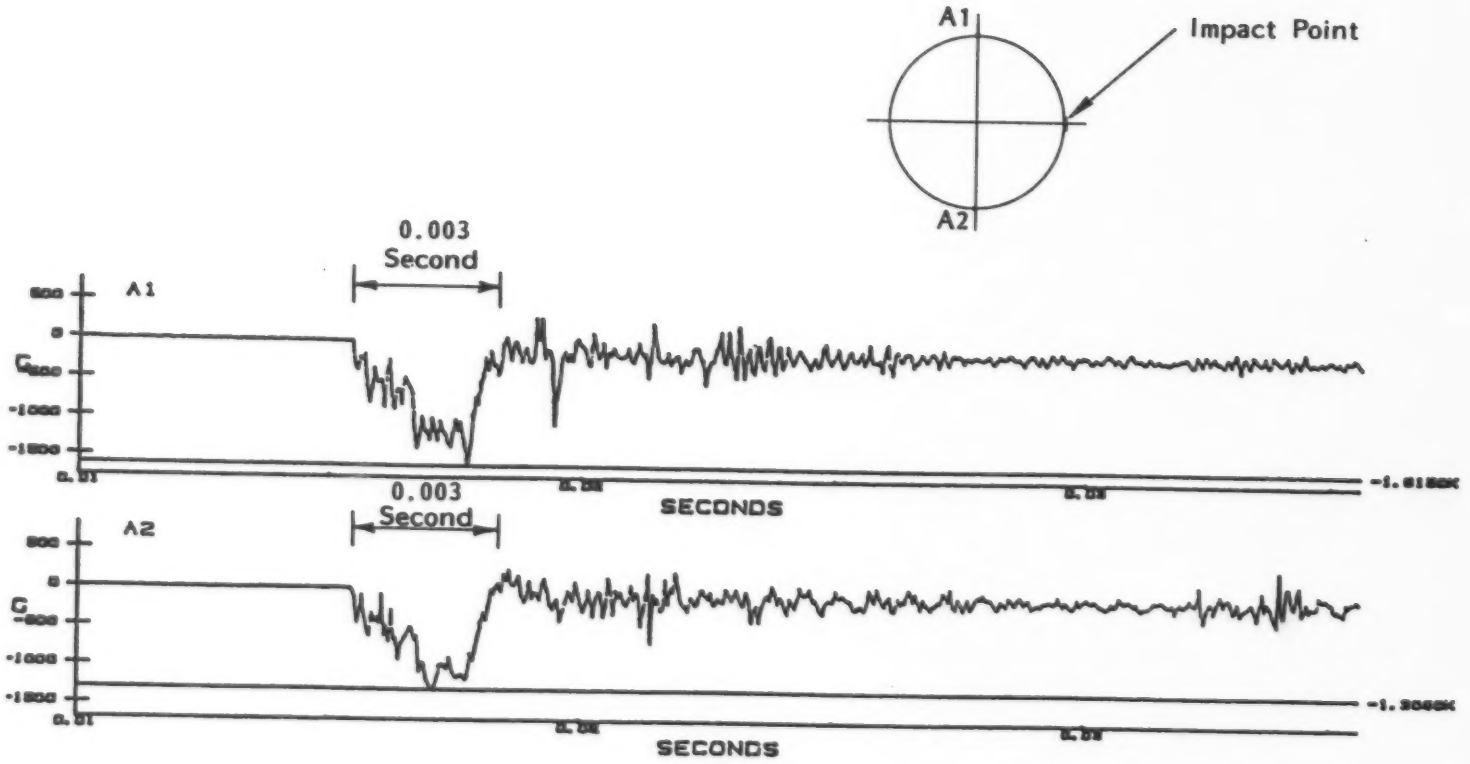

FIGURE 61

ACCELEROMETER DATA AT MID-HEIGHT OF OUTER LINER (UNITS = G's)
(1/8 SCALE MODEL)

FIGURE 62(a)

TOP CORNER DAMAGE OF 1/8 SCALE MODEL

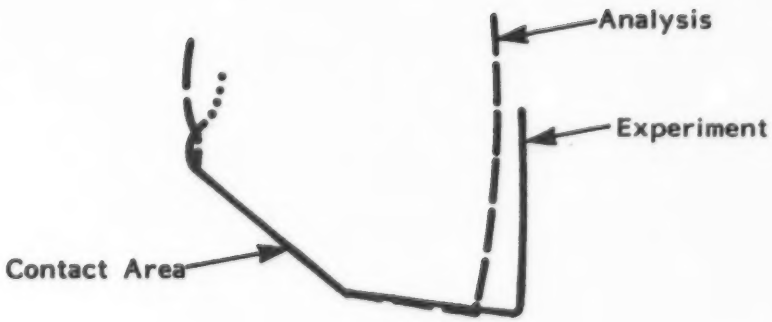

FIGURE 62(b)

COMPARISON OF TOP CORNER DEFORMATION
(1/8 SCALE MODEL)

182167-RD